Voltage Nonlinear Control in Multiterminal HVDC Networks

Luís Miguel Cabaço Nunes

Dissertation to obtain the Master of Science Degree in

Electrical and Computer Engineering

Supervisor: Prof. José Fernando Alves da Silva

Examination Committee

Chairperson: Prof. Célia Maria Santos Cardoso de Jesus
Supervisor: Prof. José Fernando Alves da Silva
Member of the Committee: Victor Manuel de Carvalho Fernão Pires

January 2021

Declaration

I declare that this document is an original work of my own authorship and it fulfils all the requirements of the Code of Conduct and Good Practices of the Universidade de Lisboa.

Acknowledgements

First, I would like to thank my supervisor Prof. José Fernando Alves da Silva, who has always been interest in this thesis and working with me. Without his guidance, knowledge, and all the excellent advices present throughout this thesis, it would be impossible to accomplish this master thesis.

I would also like to thank Instituto Superior Técnico and all my friends and colleagues, for their friendship and support. Among them, I would like to thank in a special way Afonso Godinho, Mafalda Barros, and Gonçalo Neves.

Finally, I would like to thank my family especially my parents, sister, and grandparents for their support, love, and advices. Without that, it would be much harder to conclude my master degree.

Resumo

A utilização das redes de corrente continua (DC do inglês Direct Current), incluindo a transmissão de energia em corrente contínua a alta tensão HVDC, tornou-se uma realidade nestes últimos anos, com o avanço muito acentuado da eletrónica de potência. Quando comparado com a tradicional transmissão de energia em corrente alternada a alta tensão HVAC, o sistema HVDC para longas distâncias apresenta vantagens ao nível ambiental, custo, peso, perdas, saúde pública e permite a ligação entre duas redes AC assíncronas independentes diretamente.

O objetivo desta tese é modelar e controlar uma rede DC multiterminal padrão, contendo a interligação de duas redes independentes. Cada uma destas redes é constituída por uma fonte AC, inversor-rectificador, conversor DC-DC, cargas resistivas e cargas eletrónicas, (potência constante e corrente constante). Foram criadas duas estratégias de controlo não lineares incluindo estatismo. Estes controladores têm de ser capazes de controlar a tensão da linha em regime permanente, independentemente de perturbações.

Os controladores desenvolvidos para o inversor-rectificador trifásico e para conversores DC-DC partem de dois métodos de controlo não linear baseados na teoria de estabilidade de Lyapunov, e combina a teoria do *backstepping* com a teoria do controlo por modo de deslizamento (BSMC).

Para comparação de desempenho foram desenhados e implementados controladores PI lineares na mesma rede e os resultados foram comparados com os dos controladores não lineares.

As duas estratégias referidas anteriormente foram comparadas em termos de resposta a transitórios e sobretensões/subtensões através das simulações MATLAB/Simulink. Foi possível concluir que o desempenho melhora quando se utilizam os controladores não lineares desenvolvidos.

Palavras chave: HVDC, HVAC, Rede DC multiterminal, BSMC, Controladores não lineares, Controladores Lineares.

Abstract

The use of DC networks including the transmission of energy using DC current at high voltage HVDC has become a reality with the advancement of power electronics. The HVDC system, for long distances has advantages in terms of the environment, cost, weight, losses, public health when compared to the traditional HVAC, while allowing the interconnection of two independent asynchronous AC networks directly.

The purpose of this dissertation is to model and control a standard multiterminal DC network which consists in the interconnection of two independent networks. Each of these networks have an AC source, inverter, DC-DC converter, resistive loads, and electronic loads (constant power and constant current). Two nonlinear control strategies were created including droop control. These controllers must be able to control the voltage steady state regardless of disturbances.

The developed controllers for the three-phase inverter-rectifier and for the DC-DC converters are based on two nonlinear control methods based on the theory of Lyapunov stability and combine the theory of the backstepping and the theory of sliding mode control (BSMC).

For performance assessment, linear PI controllers were designed and implemented using the network models and the results were compared with nonlinear controllers.

The two strategies mentioned above were compared in terms of response to transients and overvoltage/undervoltage through MATLAB/Simulink simulations. Results show that nonlinear controllers outperform their linear counterparts, as expected.

Keywords: HVDC, HVAC, Multiterminal DC network, BSMC, Nonlinear controllers, Linear controllers.

Table of Contents

Declaration i
Acknowledgements iii
Resumo v
Abstract vi
Table of Contents vii
List of Figures ix
List of Tables xi
List of Acronyms xii
List of Symbols xiii
Chapter 1 1
Introduction 1
1.1 Background 1
1.2 Dissertation Objectives and Motivation 2
1.3 Dissertation Structure 4
Chapter 2 5
Modelling the Standard Multiterminal DC Network 5
2.1 AC Grid Configuration 7
2.1.1 LCL Filter 7
2.1.2 Three-Phase Inverter Rectifier 12
2.2 HVDC Grid Configuration 14
2.2.1 Constant Current Load 15
2.2.2 Constant Power Load 15
2.2.3 DC-DC converter LC Output Filter 16
2.2.4 DC capacitors 17
Chapter 3 19
Control of nonlinear systems 19
3.1 Stability of Equilibrium Points 19
3.1.1 Equilibrium Points 19
3.1.2 Stability 19
3.2 Lyapunov stability 21
3.2.1 Direct method of Lyapunov 21
3.2.2 Lyapunov functions 21
3.2.3 Simple Example of Lyapunov method 22
3.3 Sliding Mode Control 23
3.4 Backstepping Controller Design 25
Chapter 4 27
Nonlinear Controllers 27
4.1 Inverter-rectifier Controllers 27
4.1.1 Nonlinear Voltage Controller of the DC-AC Converter 27
4.1.2 Power Controller 29
4.1.3 Nonlinear Current Controller of the DC-AC Converter 30
4.2 DC-DC Converter Controllers 32
4.2.1 Nonlinear Voltage Controller of the DC-DC Converter 32
4.2.2 Nonlinear Current Controller of the DC-DC Converter 33
Chapter 5 35
Multiterminal Network Linear Control 35
5.1 Linear Voltage Controller of the Inverter-Rectifier 36

5.2 Linear Controller of the DC-DC Converter 38
5.2.1 Linear Current Controller of the DC-DC Converter 38
5.2.2 Linear Voltage Controller of the DC-DC Converter 39
Chapter 6 41
Analysis of Simulation Results 41
6.1 Nonlinear Controllers Simulation Results 41
6.2 Linear Controllers Simulation Results 47
6.3 THD Analysis 53
Conclusions 57
7.1 Future Work 58
Bibliography 59
Appendix A 61

List of Figures

Figure 1.1 - Typical HVDC multi-terminal network [4] 2
Figure 1.2 - HVDC-HVAC cost [6] 2
Figure 1.3 - Equivalent circuit of a four-terminal VSC-HVDC network 3

Figure 2.1- Equivalent circuit of a four-terminal VSC-HVDC network with π model 5
Figure 2.2 – Equivalent π model of the line one 5
Figure 2.3 - Equivalent π model of the line two 6
Figure 2.4 - Equivalent π model of the line three 7
Figure 2.5 – LCL filter representation 8
Figure 2.6 – Equivalent single phase LCL filter circuit neglecting the damping resistance 8
Figure 2.7 – Equivalent single phase LCL filter circuit with the damping resistance R2´ 9
Figure 2.8 – Bode diagram without the damping resistance 10
Figure 2.9 – Bode diagram with the damping resistance 11
Figure 2.10 – AC grid representation modified from [12] 12
Figure 2.11 – Possible combinations of semiconductors [12] 13
Figure 2.12 – α, βCartesian plane modified from [12] 13
Figure 2.13 – HVDC transmission grid representation 14
Figure 2.14 – Wave forms representation 15
Figure 2.15 – Constant current load representation 15
Figure 2.16 – Constant power load representation 16
Figure 2.17 – V-I curve of constant power load and the negative impedance characteristic [13] 16
Figure 2.18 – LC filter 16

Figure 3.1 – Stability curves 20
Figure 3.2 – Asymptotically stable curve 20
Figure 3.3 – Asymptotic stability concepts [14] 20
Figure 3.4 – State functions examples [14] 22
Figure 3.5 – Closed-loop control application 23
Figure 3.6 – Typical phase portrait (SMC) [16] 24
Figure 3.7 – Typical phase portrait (SMC) with a boundary layer Δ 25

Figure 4.1 - Output inverter currents representation 27
Figure 4.2 – Nonlinear voltage controller of the inverter-rectifier representation 29
Figure 4.3 – Droop control representation 29
Figure 4.4 – Nonlinear current controller of the inverter representation 31
Figure 4.5 – Nonlinear voltage controller Simulink representation of the DC-DC converter 33
Figure 4.6 – Nonlinear current controller Simulink representation of the DC-DC converter 34

Figure 5.1 – Closed loop block diagram of a PI controller modified from [23] 35
Figure 5.2 – Step response with different coefficients [23] 36
Figure 5.3 – Closed loop block diagram of voltage modified from [21] 37
Figure 5.4 – Linear voltage controller of the inverter representation 37
Figure 5.5 – Equivalent diagram of linear current control modified from [12] 38
Figure 5.6 – Block diagram of linear current control 38
Figure 5.7 – Linear current controller of the DC-DC converter representation 39
Figure 5.8 – Block diagram of linear voltage control modified from [12] 39
Figure 5.9 – Linear voltage controller of the DC-DC converter representation 40

Figure 6.1 – Currents measured on the AC side of network one with nonlinear controller 42
Figure 6.2 – Currents measured on the AC side of network two with nonlinear controller 42
Figure 6.3 – Currents measured on the AC side of network one with nonlinear controller (zoom) 43

Figure 6.4 – Voltages measured on the AC side of network one with nonlinear controller 43
Figure 6.5 – Voltages measured on the AC side of network two with nonlinear controller..... 43
Figure 6.6 – Voltages measured on the AC side of network one with nonlinear controller (zoom)..... 44
Figure 6 7 – Voltages measured on the AC side of network one with nonlinear controller without the LCL filter (zoom) 44
Figure 6.8 – Currents measured on the output DC side of network one with nonlinear controller..... 45
Figure 6 9 – Currents measured on the output DC side of network two with nonlinear controller 45
Figure 6.10 – Currents measured on the output DC side of network one with nonlinear controller (zoom)..... 46
Figure 6.11 – Voltages measured on the DC side of network one with nonlinear controller 46
Figure 6.12 – Voltages measured on the DC side of network two with nonlinear controller..... 46
Figure 6.13 – Voltages measured on the DC side of network one with nonlinear controller without droop control 47
Figure 6.14 – Voltages measured on the DC side of network two with nonlinear controller without droop control 47
Figure 6.15 – Voltages measured on the AC side of network one with linear controller..... 48
Figure 6.16 – Voltages measured on the AC side of network two with linear controller..... 48
Figure 6.17 – Voltages measured on the AC side of network one with linear controller (zoom)..... 49
Figure 6.18 – Voltages measured on the AC side of network one with linear controller without LCL filter (zoom) 49
Figure 6.19 – Currents measured on the DC side of network one with linear controller 50
Figure 6.20 – Currents measured on the DC side of network two with linear controller 50
Figure 6.21 – Currents measured on the DC side of network one with linear controller zoom..... 50
Figure 6.22 – Voltages measured on the DC side of network one with linear controller..... 51
Figure 6.23 – Voltages measured on the DC side of network two with linear controller..... 51
Figure 6.24 – Voltages measured on the DC side of network one with linear controller without droop control .. 51
Figure 6.25 – Voltages measured on the DC side of network two with linear controller without droop control .. 52
Figure 6.26 – Vci voltage measured on the DC side of network one with linear controller (zoom)..... 52
Figure 6.27 – Vci voltage measured on the DC side of network one with nonlinear controller (zoom)..... 53
Figure 6.28 – AC Voltage FFT analysis network one using nonlinear controllers 53
Figure 6.29 – AC Voltage FFT analysis network one using linear controllers..... 54
Figure 6.30 – AC Voltage FFT analysis network two using nonlinear controllers..... 54
Figure 6.31 – AC Voltage FFT analysis network two using linear controllers..... 55
Figure 6.32 – AC current FFT analysis network one using nonlinear controllers 55
Figure 6.33 – AC current FFT analysis network two using nonlinear controllers 56

Figure A.1 – Four-terminal VSC-HVDC model with droop control and nonlinear controllers MATLAB/Simulink..... 62
Figure A.2 – Four-terminal VSC-HVDC model with droop control and linear controllers MATLAB/Simulink. 62

List of Tables

Table 2.1- γk and α, β vector table modified from [12] 14

Table 4.1 – Vector selection table 31
Table 4.2 – Truth Table of the figure 4.4 34

Table 6.1 – Simulation parameters of the inverter 41
Table 6.2 – Simulation parameters of the π line 41
Table 6.3 – Simulation parameters of the DC-DC converter 41
Table 6.4 – General gains of the PI controllers 48
Table 6.5 – PI current and voltage controllers' gains 48
Table 6.6 – THD values 56

Table A.1 – MATLAB workspace 61

List of Acronyms

AC	Alternating current
BSMC	Backstepping sliding mode controller
CLF	Control Lyapunov function
DC	Direct current
HVAC	High voltage alternating current
HVDC	High voltage direct current
PI	Proportional – Integral
RE	Renewable energy
RMS	Root mean square
SMC	Sliding mode control
THD	Total harmonic distortion
VSCs	Voltage source controllers

List of Symbols

Latin Symbols	
a_i	Gain margin of the current PI controller
a_v	Gain margin of the voltage PI controller
b_k	Polynomial coefficients
C	Capacitor DC-DC converter
C_0	Capacitor LCL filter (triangle)
C_0'	Capacitor LCL filter (star)
C_{dc}	Capacitor π line
C_i	Capacitor DC side of inverter
d	Line length
e	Error
e_I	Integral control
e_v	Voltage error
e_{V0}	Error between reference and capacitor voltage
E	Voltage
f	Grid frequency
f_c	Switching frequency
G_i	Modulation index
i	Total current equivalent single phase LCL filter
i_a	AC Phase A current
i_{ac}	AC source current equivalent single phase LCL filter
i_b	AC Phase B current
i_c	AC Phase C current
i_{C0}	Capacitor current equivalent single phase LCL filter
i_d	Current d coordinate
i_{dc}	DC current
i_q	Current q coordinate
I	Current
I_L	Inductor current
I_{Lref}	Inductor reference current
I_{L1}	π line current network 1
I_{L2}	π line current network 2
I_{L3}	π line current network 3
I_n	Nominal DC current
I_0	Output DC current
K_c	Current gain
K_d	Modulator incremental gain
K_i	Integral gain of linear voltage controller DC-DC converter
K_{ii}	Integral gain of linear current controller DC-DC converter
K_{iv}	Integral gain of linear voltage controller inverter

K_p	Proportional gain of linear voltage controller DC-DC converter
K_{pi}	Proportional gain of linear current controller DC-DC converter
K_{pv}	Proportional gain of linear voltage controller Inverter
K_v	Proportional gain of nonlinear voltage controller Inverter
K_w	Anti-windup gain
L	Inductor DC-DC converter
L_{dc}	Inductor π line
L_0	Inductor AC source
L_1	Inductor LCL filter
P	Active power
P_d	Active power d coordinate
P_q	Active power q coordinate
Q	Reactive power
r	Resistive load
r_{cpl}	Negative incremental resistance
r_{pl}	Resistive load
r_{pl1}	Resistive load
R	Resistance
R_e	Droop control
R_1	Resistance AC source
R_2	Damping resistance (triangle)
$R_2{}'$	Damping resistance (star)
R_3	Resistance LCL filter
s	Sliding surface
S	DC-DC converter semiconductor
S_{cc}	Short-circuit power
S_{1k}	Inverter semiconductor line 1
S_{2k}	Inverter semiconductor line 2
t	Time
t_d	Delay time
T	Period
T_d	Average value of t_d
T_{dv}	Delay in duty cycle
T_p	Time constant of the pole of the current PI controller
T_{pv}	Time constant of the pole of the voltage PI controller
T_z	Time constant of the zero of the current PI controller
T_{zv}	Time constant of the zero of the voltage PI controller
u	Control input
u_{ci}	Capacitor voltage
u_{ci}	Capacitor reference voltage
u_{cmax}	Upper limit of the modulating signal
U	Voltage
$\dot{V}$	Lyapunov function

V_a	AC voltage phase A
V_b	AC voltage phase B
V_c	AC voltage phase C
V_C	Capacitor voltage
V_C	Capacitor voltage
V_{Cref}	Capacitor reference voltage
V_d	Voltage d coordinate
V_i	Load output voltage
V_n	Nominal DC voltage
V_{nac}	Phase to phase Voltage
$V_{nacpeak}$	Peak Voltage
V_{nref}	Nominal DC reference voltage
V_q	Voltage q coordinate
V_0	Output DC voltage
V_0	Output DC reference voltage
W	Total energy stored on a capacitor
x_c	Capacitive reactance
X	System state vector
X_{ref}	System state reference vector
Y_t	Transverse admittance
Z_{dc}	Line impedance
Z_{RC}	Impedance of RC branch
Z_Δ	Impedance of RC branch triangle

Greek Symbols	
α_i	Current sensor gain
α_v	Voltage sensor gain
γ	DC-DC converter mode operation
γ_k	Inverter mode operation
δ	Duty-cycle
Δ	Band width
Δ_{iLmax}	Maximum current ripple
Δ_{V0}	Voltage ripple
ω_f	Resonant frequency
i_α	Current α coordinate
i_β	Current β coordinate
V_α	Voltage α coordinate
V_β	Voltage β coordinate

Chapter 1

Introduction

1.1 Background

Nowadays, the AC network is commonly used to transmit and distribute electrical energy. This methodology was adopted at the end of 19thcentury when Nikola Tesla "won" the war of currents. Back then, Tesla supported alternating current (AC) to distribute power and Thomas Edison claimed that direct current (DC) was the best and safest system for electric power distribution. At that time, AC won the battle mainly because the invention of transformers. With this important electrical machine it was possible to convert the voltage to higher or lower levels with high efficiency and lower implementation costs [1].

However, in the last years with advancement in Electronics, especially in semiconductor technology that allowed to step-up or step-down DC voltage conversion, DC networks became a possible solution to replace or complement the AC distribution system [2].

The main reason to motivate the use of DC distribution instead of AC relies in the fact that transmission capacity can be increased due to the increased voltage allowed by the low voltage directive [3]. Another important motivation is the fact that less AC/DC and DC/AC conversions are needed which improves the total efficiency of the system. Finally, is also relevant to say that DC network including the distributed energy generation provides an environment that can guarantee outage free, better power quality to consumers[3].

With the recent growth in renewable energy (RE) the DC links became more interesting, because a considerable amount of RE electricity is produced using direct current. Recent studies have shown that for long distances the best way to transmit power from offshore wind farms to the coast is by high voltage direct current (HVDC) links. This fact led a new interest in the HVDC grids, especially in the study of stability and the voltage control. In this type of RE an HVDC transmission usually results in a multi-terminal network. It is possible to control this network with voltage source converters connected in its terminals (VSCs), Fig.1.1. These converters permit the transfer of the power from the DC side to AC grids where the consumers are connected. The importance of control in this multi-terminal network is to guarantee that DC voltage remains almost stable while damping out any oscillations that results from the change in the incoming power and by faults in the AC side [4].

Multi-terminal HVDC structure brings a lot of advantages such as cost maintenance and weight reduction, but also have disadvantages. The main problem is stability in DC voltage and input filters due to the presence of the constant power loads [5].

The biggest challenge of using multi-terminal DC grid is the interconnection between the grid and electronic loads. There are three types of electronic loads, constant voltage loads that maintains the value of the voltage constant regardless the current, constant current loads that imposes a fixed current value and finally constant power loads that maintaining a constant power regardless of the line voltage are responsible for stability issues. A possible solution to overcome the stability problem, may need the insertion of a suitable capacitor in parallel to the constant-power load converter [5].

Regardless the stability issue with constant power loads, HVDC transition system is the better method to solve the problems between the interconnection of power networks, because DC power do not show frequency or phase angles incompatibilities, so it's possible to connect two separately asynchronous AC systems. For long distances HVDC system is also better because it can use underground and submarine cables. This type of system permits

more power transfer with fewer cables compared to AC system. For long distances HVAC systems have more losses than HVDC and reactive power compensation is needed and a bigger investment cost as it shown in Fig.1.2. Finally, for environment reasons HVDC is the optimal choice because it shows almost zero induction or alternating electro-magnetic fields [6].

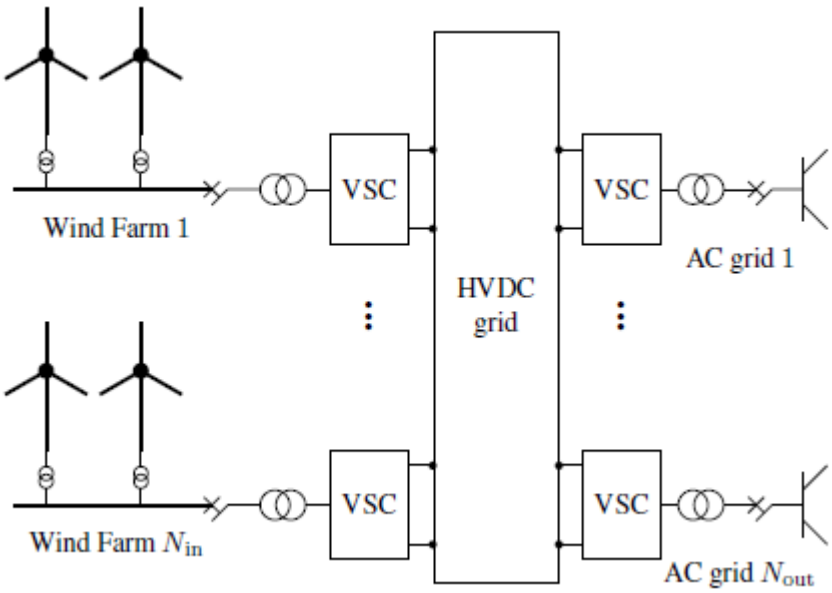

Figure 1.1 - Typical HVDC multi-terminal network [4]

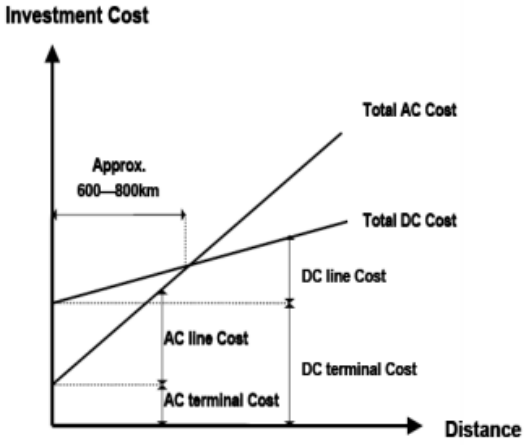

Figure 1.2 - HVDC-HVAC cost [6]

Commonly, linear controllers like proportional integral (PI) are used to regulate voltages and currents in an electronic converter. But in some cases, the use of these controllers becomes less robust against the system disturbances. To solve these cases, nonlinear controllers where developed to improve the behaviour of equipment. With nonlinear controllers such as hysteresis, sliding mode control (SMC) it is possible to control just-in time while providing a precise control action [7].

1.2 Dissertation Objectives and Motivation

This dissertation has four main objectives:

1) To derive a dynamic model for a standard multi-terminal DC network;
2) To simulate the network in a computational environment;
3) To develop control strategies for the multi-terminal DC network;

4) To evaluate the developed control strategies.

To fulfil these objectives, the standard multi-terminal DC network it will be composed by two equal circuits and a third one that connects the first ones (Fig.1.3). Basically, the system has two identical networks that are connected by a line that can be represented by a π model. Each network has a constant power load, current constant load and AC/DC, DC/DC converters. After obtaining the DC network model, the objective is to design nonlinear (and linear) controllers able to track the DC voltage at a certain value. These controllers should also guarantee the stability of all system in a way that the all network always is stable independently of the load type in use. In addition to this the second line of the DC network will have a power controller responsible for the injection of power into to the DC grid. To conclude the description of the DC network it is also relevant to refer that both grids will have low-pass filters to attenuate the amplitude of high frequency harmonics and all strategies of control the DC voltage in inverter will have droop control.

The main idea of testing both nonlinear and linear controllers is to verify if the both types have the same behaviour in similar conditions. Theoretically, it is expected that the presence of constant power loads affects the performance of the linear controllers, at least presenting larger oscillations in the DC voltage, showing probably that the best controller should be the nonlinear.

MATLAB/Simulink is the computation program chosen to carry out all the simulations and trials. The choice lies on the fact that it is an extremely reliable program in all mathematical computations, and it is recognized by all the community in this field.

One of the main purposes of this dissertation is to contribute in a significant way to develop control strategies in a DC multiterminal network because only a few works have addressed the control in this type of network. In the present years, more than ever, there is a big concern about our planet. Human activities (footprint) are responsible for the destruction of several habitats and for the greenhouse effect. Fortunately, the world community are finally doing efforts to minimize those problems and one of the solutions being implemented is the utilization of RE instead of fossil fuels. The energy produced with RE is in the DC form so the idea of use a DC network instead of using an AC one becomes more interesting.

However, just the idea isn´t enough, for that to happen the DC network must be a better solution than AC networks. As said before, considering the progress in semiconductor technology, the implementation cost, and the fact that for long distances the HVDC is advantageous regarding HVAC, makes the idea a solution for the present and future. Nevertheless, is important to refer that for the present the best way is to implement a DC multiterminal network that connects several independent grids that have AC and DC combined. For those reasons this dissertation can be an important contribute for the new and sustainable world.

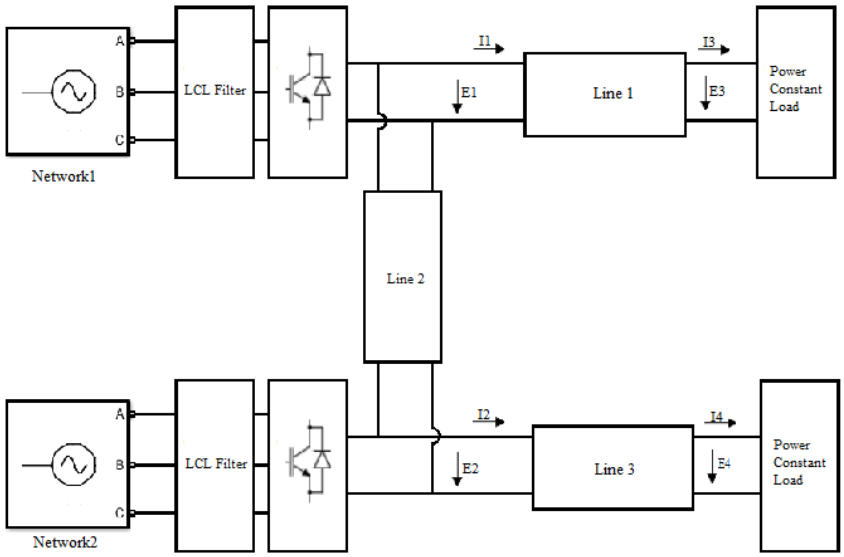

Figure 1.3 - Equivalent circuit of a four-terminal VSC-HVDC network (Constant Power Loads)

1.3 Dissertation Structure

This master dissertation is divided into seven chapters plus bibliography and appendix.

In chapter 1, the background was presented, followed by the dissertation objectives, motivation, and the dissertation structure.

In chapter 2, the dynamic model of the standard multiterminal DC network is present step-by-step together with the design of network key components.

In chapter 3, the state of art will be presented, including a brief explanation of nonlinear systems Lyapunov stability theory. Based on that, develop two nonlinear methods to design nonlinear controllers. These nonlinear methods are backstepping and sliding mode control.

In chapter 4 the objective is to design four nonlinear controllers, based on the methods explained in the previous chapter. Two of them to control voltage and current in the inverter-rectifier and the other two to control the same quantities, in the DC-DC converter (constant power loads.) This chapter also explains the power control and droop control.

In the chapter 5, linear PI theory is briefly explained and used to design controllers that control the voltages of the previous chapter. All the controllers in this chapter are linear with exception of the current controller of the inverter that is nonlinear same as in the chapter 3. These controllers are used as reference for comparison with the nonlinear controllers.

In the chapter 6, the simulations results are present and analysed using all the control approaches explained before.

In the chapter 7, the principal conclusions of this master dissertation are presented together with possible ideas for future work.

Chapter 2

Modelling the Standard Multiterminal DC Network

The standard multiterminal DC network will be modelled considering the π model of lines in Fig 1.3, shown in Fig. 2.1.

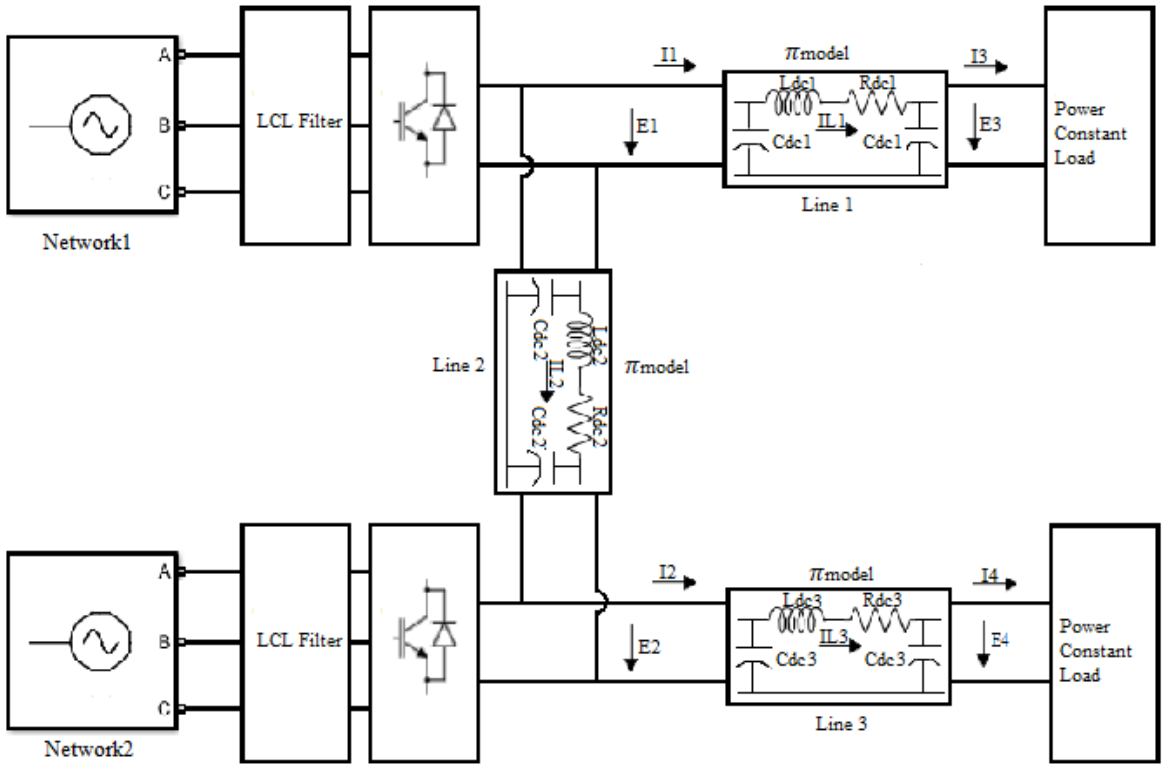

Figure 2.1- Equivalent circuit of a four-terminal VSC-HVDC network with π model

In the Fig 2.1 the DC lines are modelled by an equivalent circuit of four terminals. For the analysis each one of the three-line equivalent circuits will be considered separately. For each one of the tree line equivalent circuits the model equations are represented hereafter.

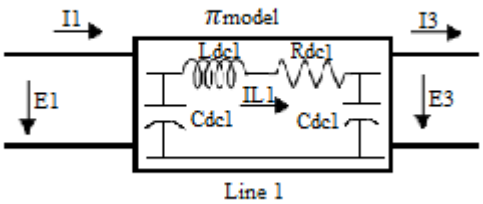

Figure 2.2 – Equivalent π model of the line one

The equations of the equivalent π model of the line one (Fig. 2.1) are:

$$\begin{bmatrix} E_1 \\ I_1 \end{bmatrix} = \begin{bmatrix} 1 + Z_{dc1}\frac{Y_T}{2} & Z_{dc1} \\ Y_T\left(1 + Z_{dc1}\frac{Y_T}{4}\right) & 1 + Z_{dc1}\frac{Y_T}{2} \end{bmatrix} \begin{bmatrix} E_3 \\ I_3 \end{bmatrix} \tag{2.1}$$

Or:

$$\begin{bmatrix} E_3 \\ I_3 \end{bmatrix} = \begin{bmatrix} 1 + Z_{dc1}\frac{Y_T}{2} & -Z_{dc1} \\ -Y_T\left(1 + Z_{dc1}\frac{Y_T}{4}\right) & 1 + Z_{dc1}\frac{Y_T}{2} \end{bmatrix} \begin{bmatrix} E_1 \\ I_1 \end{bmatrix} \tag{2.2}$$

Where:

$$Z_{dc1} = R_{dc1} + jL_{dc1} \tag{2.3}$$

$$\frac{Y_T}{2} = \text{Transverse admittance} \tag{2.4}$$

$$I_{L_1} = \frac{E_1 - E_3}{Z_{dc1}} \tag{2.5}$$

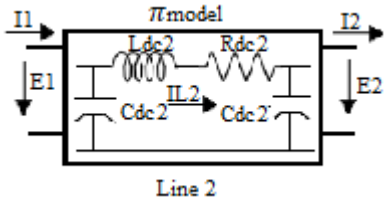

Figure 2.3 - Equivalent π model of the line two

The equations of the equivalent π model of the line two (Fig. 2.3) are:

$$\begin{bmatrix} E_1 \\ I_1 \end{bmatrix} = \begin{bmatrix} 1 + Z_{dc2}\frac{Y_T}{2} & Z_{dc2} \\ Y_T\left(1 + Z_{dc2}\frac{Y_T}{4}\right) & 1 + Z_{dc2}\frac{Y_T}{2} \end{bmatrix} \begin{bmatrix} E_2 \\ I_2 \end{bmatrix} \tag{2.6}$$

Or:

$$\begin{bmatrix} E_2 \\ I_2 \end{bmatrix} = \begin{bmatrix} 1 + Z_{dc2}\frac{Y_T}{2} & -Z_{dc2} \\ -Y_T\left(1 + Z_{dc2}\frac{Y_T}{4}\right) & 1 + Z_{dc2}\frac{Y_T}{2} \end{bmatrix} \begin{bmatrix} E_1 \\ I_1 \end{bmatrix} \tag{2.7}$$

Where:

$$I_{L_2} = \frac{E_1 - E_2}{Z_{dc2}} \tag{2.8}$$
$$Z_{dc2} = R_{dc2} + jL_{dc2}$$

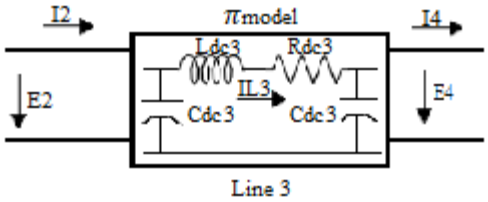

Figure 2.4 - Equivalent π model of the line three

The equations of the equivalent π model of the line three (Fig.2.4) are:

$$\begin{bmatrix} E_2 \\ I_2 \end{bmatrix} = \begin{bmatrix} 1 + Z_{dc3}\frac{Y_T}{2} & Z_{dc3} \\ Y_T\left(1 + Z_{dc3}\frac{Y_T}{4}\right) & 1 + Z_{dc3}\frac{Y_T}{2} \end{bmatrix} \begin{bmatrix} E_4 \\ I_4 \end{bmatrix} \tag{2.9}$$

Or:

$$\begin{bmatrix} E_4 \\ I_4 \end{bmatrix} = \begin{bmatrix} 1 + Z_{dc3}\frac{Y_T}{2} & -Z_{dc3} \\ -Y_T\left(1 + Z_{dc3}\frac{Y_T}{4}\right) & 1 + Z_{dc3}\frac{Y_T}{2} \end{bmatrix} \begin{bmatrix} E_2 \\ I_2 \end{bmatrix} \tag{2.10}$$

Where:

$$I_{L_3} = \frac{E_2 - E_4}{Z_{dc3}}$$
$$Z_{dc3} = R_{dc3} + jL_{dc3} \tag{2.11}$$

The above equations are used in the simulations of the multiterminal network lines.

2.1 AC Grid Configuration

For the purpose of this dissertation the AC side powering the DC grids will be represented by a three-phase system with internal short-circuit impedance connected to a 3-phase inverter-rectifier. The AC sources short circuit resistive and inductive components of the impedances cannot be neglected due to the power levels transmitted. These sources are connected to inverter-rectifiers in the multiterminal HVDC system. The inverter-rectifier switching action injects high frequency harmonics in the current waveforms. The amplitude of the harmonics decreases with the harmonic order relative to the switching frequency but still require to be further attenuated. Therefore, in the AC side the use of a filter that acts like a low pass-filters to minimize the harmonics amplitude especially in high frequencies is required. LCL filter is going to be used instead of a traditional LC filter because presents a better performance in this type of system.

2.1.1 LCL Filter

The high frequency harmonics produced by the inverter-rectifier may cause ripple in the power system variables. The ripple can create resonance problems at the harmonic frequencies [8]. Therefore, the design and utilization of an AC filter is crucial to minimize the harmonics problems. The AC filter basically acts as a low-pass filter. This filter is installed between the three-phase voltage source and the inverter-rectifier. Thus, the high frequencies are strongly attenuated, while the fundamental harmonic are almost not affected [9]. The filter has a T shape with two inductors (and their parasitic resistances) and a capacitor in series with a damping resistance connected in a triangle form (Fig.2.5). The use of high order LCL filter improves the attenuation in the high frequencies compared to the traditional LC filter. The weight and size of the LCL components are reduced, using smaller values of inductors and capacitors while guaranteeing a good performance [10].

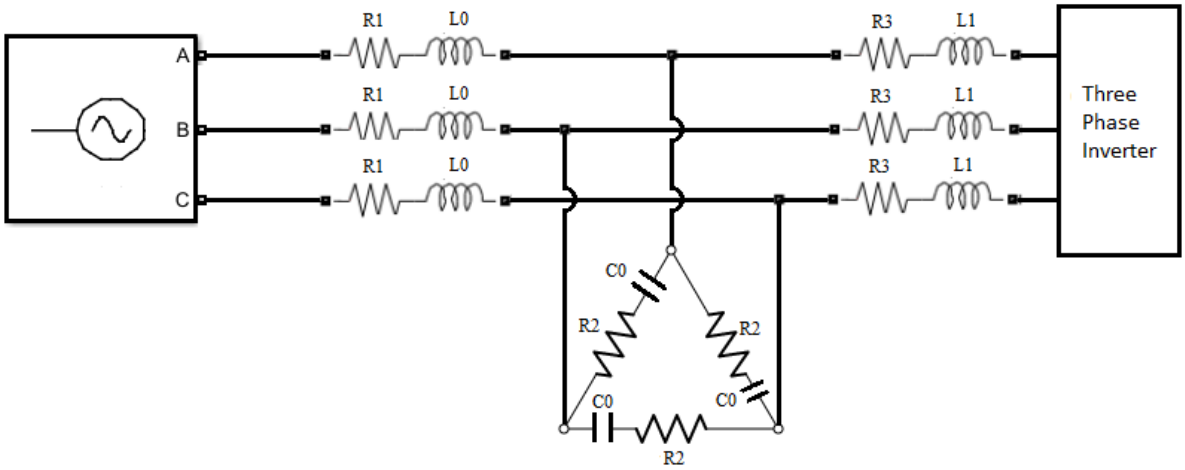

Figure 2.5 – LCL filter representation

To size the filter inductance values it is considered an equivalent single phase LCL filter circuit (Fig 2.6) in which the damping resistance is neglected.

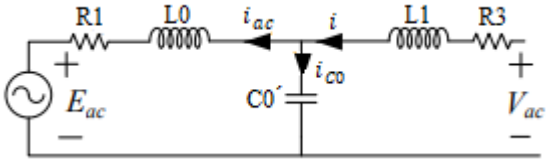

Figure 2.6 – Equivalent single phase LCL filter circuit neglecting the damping resistance

The dynamic behaviour of the circuit (Fig 2.6) can be described in the following form:

$$\begin{cases} \dfrac{dv_{C0'}}{dt} = \dfrac{1}{C_0'}(i - i_{ac}) \\ \dfrac{di}{dt} = \dfrac{1}{L_1}(V_{ac} - v_{C0'} - R_3 i) \\ \dfrac{di_{ac}}{dt} = \dfrac{1}{L_0}(v_{C0'} - E_{ac} - R_1 i_{ac}) \end{cases} \tag{2.12}$$

Rewriting the 2.12 into matrix form to obtain the state model $\dot{x} = Ax + Bu$

$$\begin{bmatrix} \dfrac{di}{dt} \\ \dfrac{di_{ac}}{dt} \\ \dfrac{dv_{C0'}}{dt} \end{bmatrix} = \begin{bmatrix} -\dfrac{R_3}{L_1} & 0 & -\dfrac{1}{L_1} \\ 0 & -\dfrac{R_1}{L_0} & \dfrac{1}{L_0} \\ \dfrac{1}{C_0'} & -\dfrac{1}{C_0'} & 0 \end{bmatrix} \begin{bmatrix} i \\ i_{ac} \\ v_{C0'} \end{bmatrix} + \begin{bmatrix} \dfrac{1}{L_1} & 0 \\ 0 & -\dfrac{1}{L_0} \\ 0 & 0 \end{bmatrix} \begin{bmatrix} V_{ac} \\ E_{ac} \end{bmatrix} \tag{2.13}$$

$$A = \begin{bmatrix} -\dfrac{R_3}{L_1} & 0 & -\dfrac{1}{L_1} \\ 0 & -\dfrac{R_1}{L_0} & \dfrac{1}{L_0} \\ \dfrac{1}{C_0'} & -\dfrac{1}{C_0'} & 0 \end{bmatrix}, B = \begin{bmatrix} \dfrac{1}{L_1} & 0 \\ 0 & -\dfrac{1}{L_0} \\ 0 & 0 \end{bmatrix} \tag{2.14}$$

The filter transfer function is the following:

$$\frac{I_{ac}(s)}{V_{ac}(s)} = \frac{1}{(L_1 L_0 C_0')s^3 + as^2 + bs + (R_3 + R_1)} \tag{2.15}$$

Where,

$$a = L_1 C_0{}' R_1 + L_0 C_0{}' R_3$$
$$b = C_0{}' R_3 R_1 + L_1 + L_0 \quad (2.16)$$

The denominator of the transfer function (2.15) can be factorized into two factors as demonstrated in (2.17).

$$\frac{I_{ac}(s)}{V_{ac}(s)} = \frac{c}{(1+sd)(1+b_1 s + a_1 s^2)} \quad (2.17)$$

Where,

$$c = \frac{1}{R_3 + R_1}$$
$$d = \frac{C_0{}' R_3 R_1 + L_1 + L_0}{R_3 + R_1}$$
$$b_1 = \frac{L_1 C_0{}' R_1 + L_0 C_0{}' R_3}{C_0{}' R_3 R_1 + L_1 + L_0} \quad (2.18)$$
$$a_1 = \frac{L_1 L_0 C_0{}'}{C_0{}' R_3 R_1 + L_1 + L_0}$$

From the second order term the resonant frequency of the circuit can be written in the following form:

$$\omega_f = \sqrt{\frac{C_0{}' R_3 R_1 + L_1 + L_0}{L_1 L_0 C_0{}'}} \quad (2.19)$$

If the resistances of inductances are neglected the resonant frequency is expressed in the following form:

$$\omega_f = \sqrt{\frac{L_1 + L_0}{L_1 L_0 C_0{}'}} \quad (2.20)$$

Taking into account (2.20) the capacitor C_0 is expressed in the following form:

$$C_0{}' = \frac{L_0 + L_1}{L_1 L_0 {\omega_f}^2} \quad (2.21)$$

To smooth the overall response a resistance in series with filter capacitance is placed to damp out resonance, this resistance ($R_2{}'$) behaves like a passive damping (Fig. 2.7). The $R_2{}'$ in series with $C_0{}'$ attenuates the gain and improve the stability of the system.

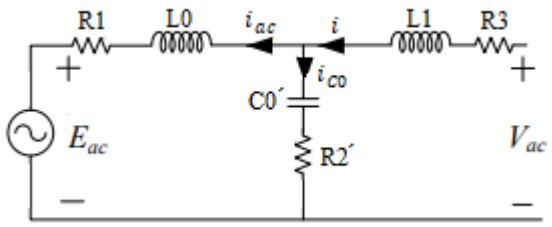

Figure 2.7 – Equivalent single phase LCL filter circuit with the damping resistance R2´

The dynamic behaviour of the circuit (Fig. 2.7) can be described in the following form:

$$\begin{cases} \dfrac{dv_{C0'}}{dt} = \dfrac{1}{C_0'}(i - i_{ac}) \\ \dfrac{di}{dt} = \dfrac{1}{L_1}\left(V_{ac} - v_{C0'} - R_3 i - R_2'(i - i_{ac})\right) \\ \dfrac{di_{ac}}{dt} = \dfrac{1}{L_0}\left(v_{C0'} - E_{dc} - R_1 i_{ac} + R_2'(i - i_{ac})\right) \end{cases} \tag{2.22}$$

Rewriting the 2.22 into matrix form to obtain the state model $\dot{x} = Ax + Bu$

$$\begin{bmatrix} \dfrac{di}{dt} \\ \dfrac{di_{ac}}{dt} \\ \dfrac{dv_{C0'}}{dt} \end{bmatrix} = \begin{bmatrix} -\dfrac{R_3 + R_2'}{L_1} & \dfrac{R_2'}{L_1} & -\dfrac{1}{L_1} \\ \dfrac{R_2'}{L_0} & -\dfrac{R_1 + R_2'}{L_0} & \dfrac{1}{L_0} \\ \dfrac{1}{C_0'} & -\dfrac{1}{C_0'} & 0 \end{bmatrix} \begin{bmatrix} i \\ i_{ac} \\ v_{C0}' \end{bmatrix} + \begin{bmatrix} \dfrac{1}{L_1} & 0 \\ 0 & -\dfrac{1}{L_0} \\ 0 & 0 \end{bmatrix} \begin{bmatrix} V_{ac} \\ E_{ac} \end{bmatrix} \tag{2.23}$$

$$A = \begin{bmatrix} -\dfrac{R_3 + R_2'}{L_1} & \dfrac{R_2'}{L_1} & -\dfrac{1}{L_1} \\ \dfrac{R_2'}{L_0} & -\dfrac{R_1 + R_2'}{L_0} & \dfrac{1}{L_0} \\ \dfrac{1}{C_0'} & -\dfrac{1}{C_0'} & 0 \end{bmatrix}, B = \begin{bmatrix} \dfrac{1}{L_1} & 0 \\ 0 & -\dfrac{1}{L_0} \\ 0 & 0 \end{bmatrix} \tag{2.24}$$

The filter transfer function with the damping resistance is the following:

$$\frac{I(s)}{V_{ac}(s)} = \frac{(L_0 C_0')s^2 + (R_1 C_0' + R_2' C_0')s + 1}{(L_1 L_0 C_0')s^3 + a_2 s^2 + b_2 s + (R_1 + R_3)} \tag{2.25}$$

Where,

$$\begin{aligned} a_2 &= L_0 C_0' R_3 + L_1 R_1 C_0' + L_1 R_2' C_0' + L_0 R_2' C_0' \\ b_2 &= R_3 R_1 C_0' + L_1 + R_3 R_2' C_0' + L_0 + R_2' C_0' R_1 \end{aligned} \tag{2.26}$$

The value of the resistance R_2' can be defined as follows:

$$R_2' = \frac{1}{\omega_f C_0} \tag{2.27}$$

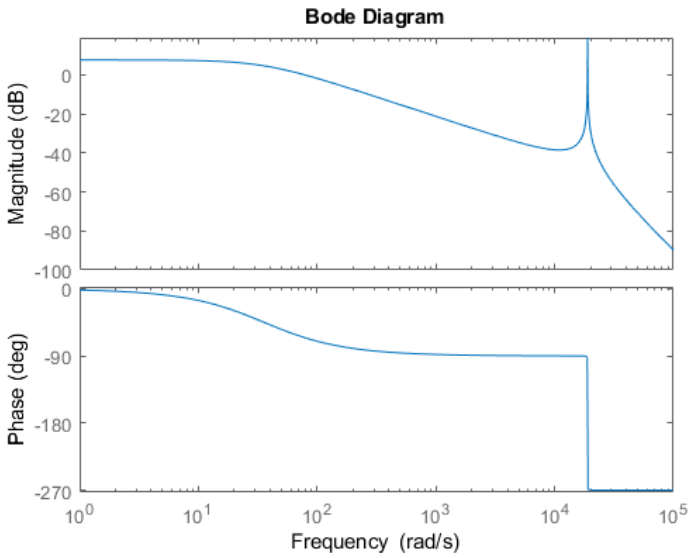

Figure 2.8 – Bode diagram without the damping resistance

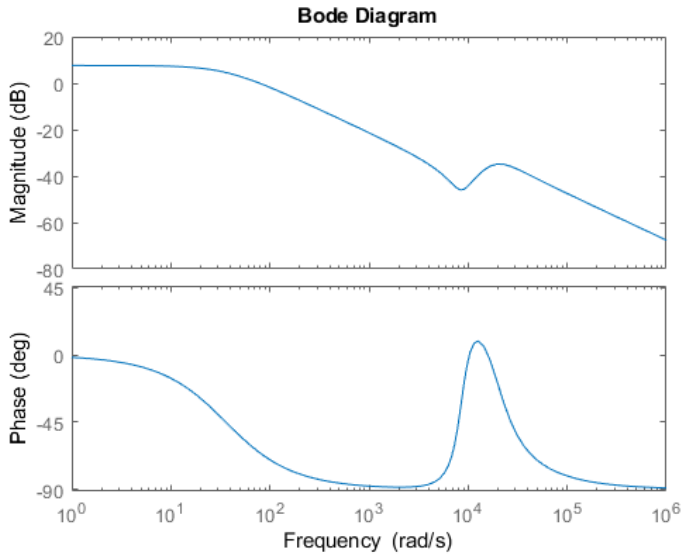

Figure 2.9 – Bode diagram with the damping resistance

Comparing the bode diagram of figures 2.8 and 2.9 is possible to observe that including the damping resistance the gain at the resonant frequency is strongly reduced.

The impedance of a RC branch is defined as follows:

$$Z_{RC} = R - j\frac{1}{x_C} \tag{2.28}$$

However, the RC filter in the figure 2.5 is connected in a triangle form being defined as $Z_{\triangle} = 3Z_{RC}$ where, Z_{RC} is connected in star form.

Therefore, the filter RC in triangle form will be defined as:

$$C_0 = \frac{L_0 + L_1}{3\left(L_1 L_0 {\omega_f}^2\right)} \tag{2.29}$$

$$R_2 = \frac{3}{\omega_f C_0}$$

Considering the Fig. 2.5 the internal impedance of the AC can be written in the following form [11]:

$$L_0 = \frac{{V_{nac}}^2}{S_{cc}}\frac{1}{\omega} \tag{2.30}$$

$$R_1 = \frac{\omega L_0}{7} \tag{2.31}$$

Where L_0 and R_1 are the internal impedance of the AC source, V_{nac} is the phase-to-phase voltage, S_{cc} is the short-circuit power, ω is angular frequency of the network, and X/R ratio = 7.

The maximum current ripple of the inverter-rectifier is given by [12]:

$$\Delta i_{Lmax} = \frac{V_n}{3\left(L_{eq}\right)}\delta T \tag{2.32}$$

Where L_{eq} is the equivalent inductor filter, δ is the duty-cycle, Δi_{Lmax} is the ripple of the current, V_n is the nominal DC voltage, T is the period.

The current that goes to the RC branch is very low so the inductors L_0 and L_1 are practically in series. Hence, the L_{eq} is approximately equal to the sum of L_0 and L_1 (2.33), with that is possible to reduce the filter size.

$$L_{eq} = L_0 + L_1 \tag{2.33}$$

The maximum peak-to-peak current ripple happens at $\delta = 0.5$, then [12]:

$$\Delta i_{Lmax} = \frac{V_n}{6(L_1 + L_0)} T \tag{2.34}$$

From (2.34) the expression of L_1 is given by:

$$L_1 = \frac{V_n}{6\Delta i_{Lmax}} T - L_0 \tag{2.35}$$

$$R_3 = 0.01\Omega \tag{2.36}$$

Where, R_3 is the resistance connected in series with the inductor L_1 and its value is computed considering the efficiency of the inverter-rectifier and the losses. The current ripple will be 10% of the inductor L_1 current ($\Delta i_{Lmax} = 0.1 I_{L1}$). The current I_{L1} is computed assuming a near unity efficiency in the inverter-rectifier. Hence, the I_{L1} is computed as follows:

$$I_{L1} = \frac{V_n I_n}{\sqrt{3} V_{nac}} \tag{2.37}$$

2.1.2 Three-Phase Inverter Rectifier

To model the inverter-rectifier shown in the Fig. 2.10 it is assumed the L_{eq} is approximately equal to the sum of L_0 and L_1, so that the LCL filter is seen as an RL circuit by the inverter-rectifier.

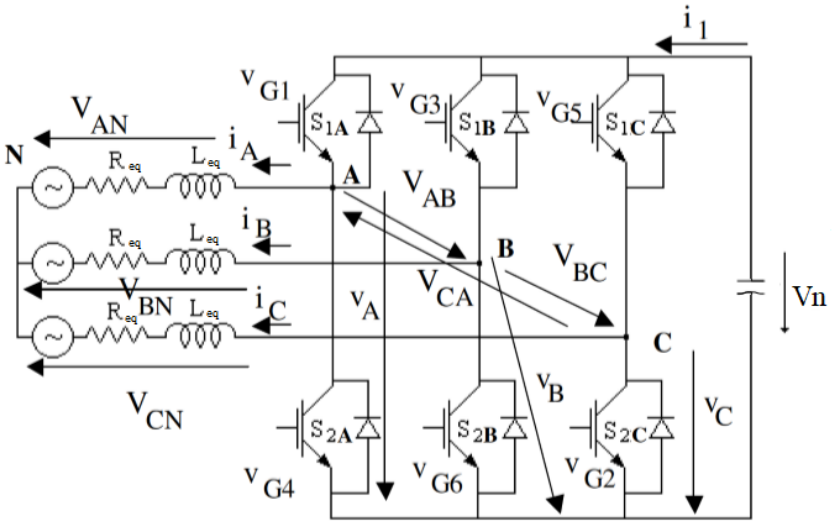

Figure 2.10 – AC grid representation modified from [12]

Each inverter branch can be controlled using a binary variable γ_k to define the branch status.

$$\gamma_k = \begin{cases} 1 \rightarrow S_{1k}\ ON \wedge S_{2k}\ OFF \\ 0 \rightarrow S_{1k}\ OFF \wedge S_{2k}\ ON \end{cases}, k \in \{A, B, C\} \tag{2.38}$$

$$V_k = \gamma_k V_n \tag{2.39}$$

From Fig. 2.11 is possible to see all the possible combinations of the semiconductors.

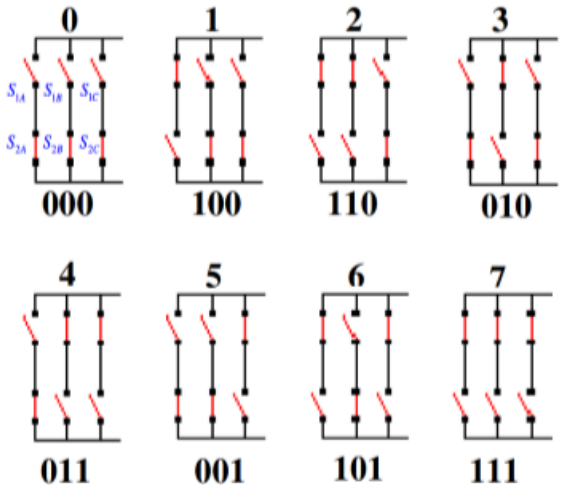

Figure 2.11 – Possible combinations of semiconductors [12]

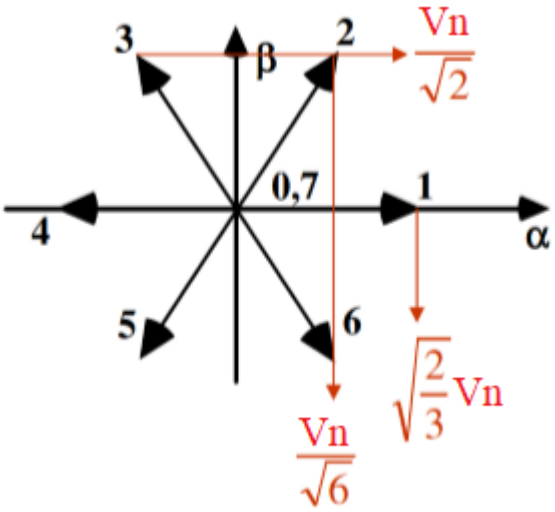

Figure 2.12 – α, β Cartesian plane modified from [12]

To fully understand the operation mode of the inverter is necessary to build the following table with γ_k and α, β notation. The table 2.1 was build considering the Fig. 2.12 and the (2.40) equation [12].

$$V_{AN} = \frac{(2\gamma_A - \gamma_B - \gamma_C)V_n}{3}$$
$$V_{BN} = \frac{(2\gamma_B - \gamma_C - \gamma_A)V_n}{3} \quad (2.40)$$
$$V_{CN} = \frac{(2\gamma_C - \gamma_A - \gamma_B)V_n}{3}$$

Table 2.1 - γ_k and α, β vector table modified from [12]

Vetor	γ_A	γ_B	γ_C	V_{AN}	V_{BN}	V_{CN}	V_α	V_β
0	0	0	0	0	0	0	0	0
1	1	0	0	$\frac{2V_n}{3}$	$-\frac{V_n}{3}$	$-\frac{V_n}{3}$	$\sqrt{\frac{2}{3}}V_n$	0
2	1	1	0	$\frac{V_n}{3}$	$\frac{V_n}{3}$	$-\frac{2V_n}{3}$	$\frac{V_n}{\sqrt{6}}$	$\frac{V_n}{\sqrt{2}}$
3	0	1	0	$-\frac{V_n}{3}$	$\frac{2V_n}{3}$	$-\frac{V_n}{3}$	$-\frac{V_n}{\sqrt{6}}$	$\frac{V_n}{\sqrt{2}}$
4	0	1	1	$-\frac{2V_n}{3}$	$\frac{V_n}{3}$	$\frac{V_n}{3}$	$-\sqrt{\frac{2}{3}}V_n$	0
5	0	0	1	$-\frac{V_n}{3}$	$-\frac{V_n}{3}$	$\frac{2V_n}{3}$	$-\frac{V_n}{\sqrt{6}}$	$-\frac{V_n}{\sqrt{2}}$
6	1	0	1	$\frac{V_n}{3}$	$-\frac{2V_n}{3}$	$\frac{V_n}{3}$	$\frac{V_n}{\sqrt{6}}$	$-\frac{V_n}{\sqrt{2}}$
7	1	1	1	0	0	0	0	0

The V_α,V_β matrix is given by the transformation matrix Clark-Concordia:

$$\begin{bmatrix} V_\alpha \\ V_\beta \\ V_0 \end{bmatrix} = \sqrt{\frac{2}{3}} \begin{bmatrix} 1 & -\frac{1}{2} & -\frac{1}{2} \\ 0 & \frac{\sqrt{3}}{2} & -\frac{\sqrt{3}}{2} \\ \frac{1}{\sqrt{2}} & \frac{1}{\sqrt{2}} & \frac{1}{\sqrt{2}} \end{bmatrix} \begin{bmatrix} V_{AN} \\ V_{BN} \\ V_{CN} \end{bmatrix} \tag{2.41}$$

The transformation matrix that allows the conversion$\alpha\beta$to ABC is the following:

$$\begin{bmatrix} V_a \\ V_b \\ V_c \end{bmatrix} = \begin{bmatrix} 1 & 0 & \frac{1}{\sqrt{2}} \\ -\frac{1}{2} & \frac{\sqrt{3}}{2} & \frac{1}{\sqrt{2}} \\ -\frac{1}{2} & -\frac{\sqrt{3}}{2} & \frac{1}{\sqrt{2}} \end{bmatrix} \begin{bmatrix} V_\alpha \\ V_\beta \\ V_0 \end{bmatrix} \tag{2.42}$$

2.2 HVDC Grid Configuration

The HVDC transmission grid will be loaded by constant power loads and with DC-DC converters feeding constant current loads.

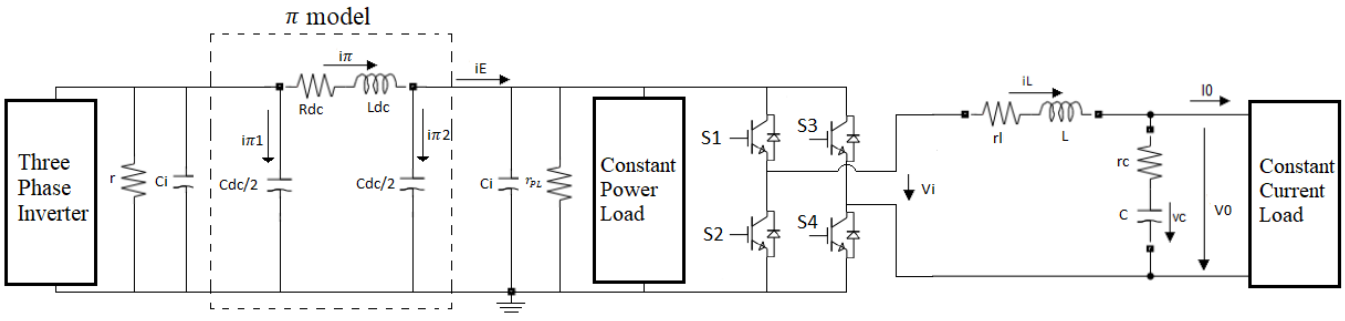

Figure 2.13 – HVDC transmission grid representation

The DC-DC converter (Fig. 2.13) is here illustrated with a four-quadrant chopper, because this converter has three operating modes:

$$\gamma = \begin{cases} 1, & If\ S1\ \wedge\ S4\ ON \\ 0, & \begin{cases} If\ S1\ \wedge\ S3\ ON \\ If\ S2\ \wedge\ S4\ ON \end{cases} \\ -1, & If\ S2\ \wedge\ S3\ ON \end{cases} \tag{2.43}$$

$$V_i = \gamma U = \begin{cases} +U \\ 0 \\ -U \end{cases} \tag{2.44}$$

Fig. 2.14 shows an example of the V_i waveform, while the DC output current is assumed nearly constant.

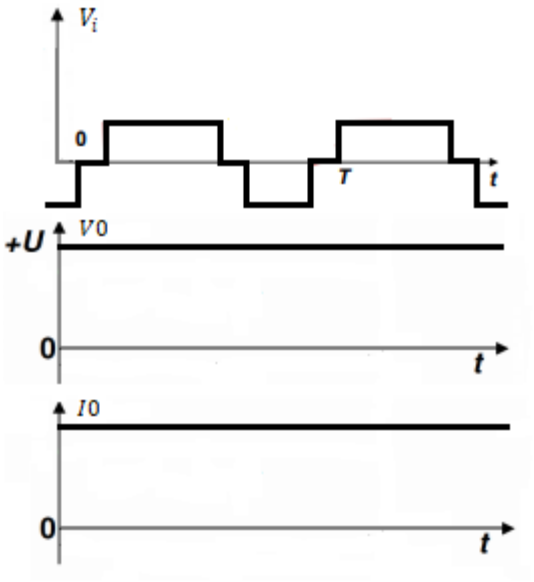

Figure 2.14 – Wave forms representation

2.2.1 Constant Current Load

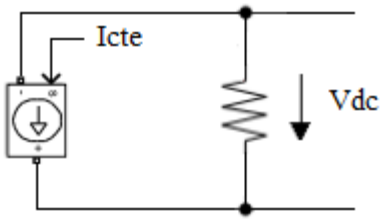

Figure 2.15 – Constant current load representation

From Fig. 2.15, supposing the load resistor is big enough to absorb negligible power, the load power P is:

$$P = V_{dc} I_{cte} \tag{2.45}$$

The load power P depends on the value of I_{cte} in (2.45).

2.2.2 Constant Power Load

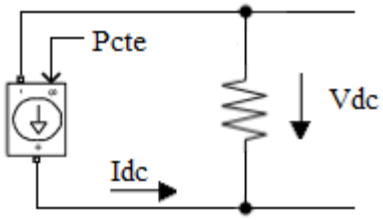

Figure 2.16 – Constant power load representation

From Fig. 2.16, supposing the represented resistor is big enough to absorb negligible power, the load constant power P is:

$$P_{cte} = I_{dc}V_{dc} = constante \tag{2.46}$$

For constant P_{cte}, the load current is obtained solving (2.46) for I_{dc}.

Constant power load exhibit negative incremental resistance (2.47) and this behaviour is the responsible for stability issues in transmission lines [13].

$$dP_{cte} = V_{dc}dI_{dc} + I_{dc}dV_{dc} = 0 \Leftrightarrow \frac{V_{dc}}{I_{dc}} = \frac{dV_{dc}}{dI_{dc}} = -r_{cpl} \tag{2.47}$$

As it shown in Fig. 2.17 the voltage decreases with increase in current and vice-versa. The negative impedance characteristic of constant power load is also shown.

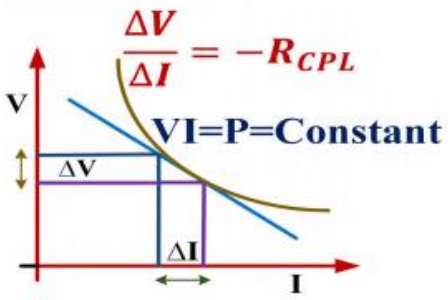

Figure 2.17 – V-I curve of constant power load and the negative impedance characteristic [13]

2.2.3 DC-DC converter LC Output Filter

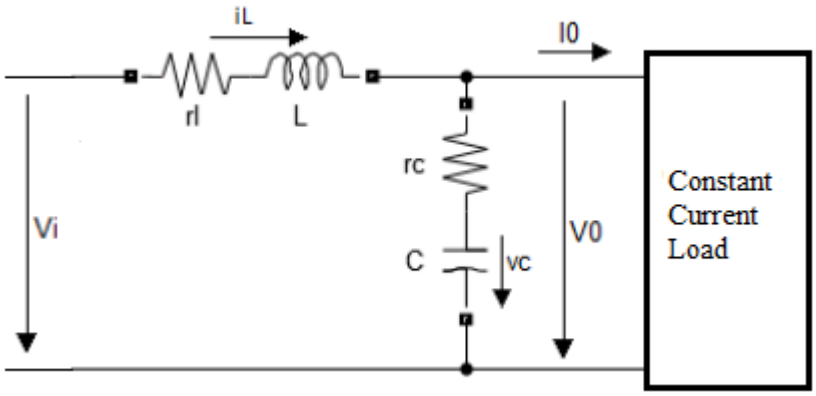

Figure 2.18 – LC filter

The Fig. 2.18 represents the output filtering stage of the DC-DC converter. The dynamical behaviour of the output filter capacitor voltage V_0 can be described by the following equations.

$$\begin{cases} C\dfrac{dV_0}{dt} = i_L - I_0 \\ L\dfrac{di_L}{dt} = V_i - V_0 \end{cases} \tag{2.48}$$

In order to have a proper LC filter the equations in the section four quadrant chopper LC filtering of [12] are used.

$$L = \frac{V_n}{4\Delta i_{Lmax}} T \tag{2.49}$$

$$C = \frac{V_n}{32L\Delta V_0} T^2 \tag{2.50}$$

Where L is the inductor filter, C is the capacitor filter, Δi_{Lmax} is the ripple of the current, V_n is the nominal DC voltage, T is the switching period, $\Delta V_0$is the voltage ripple.

2.2.4 DC capacitors

The DC capacitors act as energy storage and because of that they play a very important role in the HVDC network. The size of the capacitors determines the dynamic behaviour of the DC circuit [9].

The instantaneous energy stored in a capacitor *C* charged with voltage v_C is given by:

$$W(v_C) = \frac{1}{2} C {v_C}^2 \tag{2.51}$$

The capacitance value can be estimated, allowing a certain small voltage ripple Δv_C:

$$C \approx \frac{I_0 T}{4\Delta v_c} \tag{2.52}$$

Chapter 3

Control of nonlinear systems

The main objective of this chapter is to explain in a simplified and summarized form some different techniques to control nonlinear systems.

Nonlinear systems are characterized by the absence of a unifying property, so it is not possible to have a general and unifying theory [14]. There are many examples of a nonlinear systems, such as, solar collector thermal plants, chemical reactors, robot arms, phase modulation communication systems, switching power converters and other examples with interest in engineering field. Whenever there are wide changes in the operating point, the system presents a nonlinear behaviour. There are some systems whose behaviour can only be understood considering its nonlinear character, an example of this is meteorology. Nonlinear systems may have a specific characteristic, such as, the possibility of more than one solution, multiple isolated equilibrium points and singularities in the time response. However, the purpose of studying nonlinear controllers is to understand techniques to maintain the non-linear system stable, as the main objective of a control a system is to guarantee stability.

3.1 Stability of Equilibrium Points

For nonlinear systems the notions of equilibrium points and stability are connected through the linearization procedure. Linearization consists of obtaining a linear model [14].

3.1.1 Equilibrium Points

A nonlinear system can have multiple equilibrium points, an example of that is the following:

$$\dot{x}_1 = x_1 - x_2 \tag{3.1}$$

$$\dot{x}_2 = 4 - x_1 x_2 \tag{3.2}$$

To find out the equilibrium points the following system of equations must be solved:

$$\begin{cases} x_1 - x_2 = 0 \\ 4 - x_1 x_2 = 0 \end{cases} \tag{3.3}$$

The solution of (3.3) have two equilibrium points

$$x_A = \begin{bmatrix} 2 \\ 2 \end{bmatrix} \text{ e } x_B = \begin{bmatrix} -2 \\ -2 \end{bmatrix} \tag{3.4}$$

With this simple example it is possible to understand that nonlinear systems can have multiple equilibrium points.

3.1.2 Stability

Aleksandr Mikhailovich Lyapunov (1857-1918) was a Russian physicist and mathematician who played a crucial role in the study of the stability of dynamic systems.

The best way to define stability is to use the definition of Lyapunov. To define stability in Lyapunov sense it is necessary to consider the following differential equation:

$$\dot{x} = f(x) \tag{3.5}$$

In Lyapunov sense the state of equilibrium $x = 0$ the (3.5) is said to be stable if for any $R > 0$ there exists $r > 0$ such that if $\|x(0)\| < r$ then $\|x(0)\| < R$ for all $t \geq 0$. Otherwise the state of equilibrium is said to be unstable (Fig. 3.1).

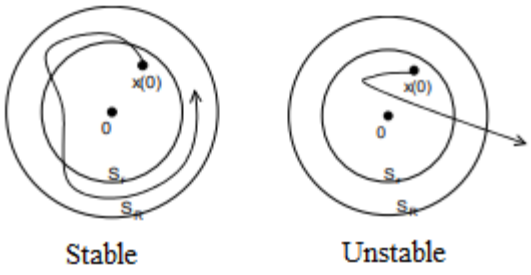

Figure 3.1 – Stability curves

The equilibrium point can also be characterized as asymptotically stable if the following definition is verified.

The equilibrium point $x = 0$ the (3.5) is asymptotically stable if it is stable and, besides that, if there exists $r > 0$ such that $\|x(0)\| < r$ implies $x(t) \to 0$ when $t \to \infty$.

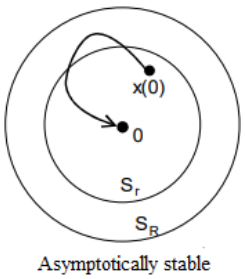

Figure 3.2 – Asymptotically stable curve

This definition concerns the local behaviour of the system, in other words, the behaviour of state when it is initialized "close" to the equilibrium point (Fig. 3.2) [14].

If asymptotic stability is valid for any initial state, then the equilibrium point is said to be globally asymptotically stable (Fig. 3.3).

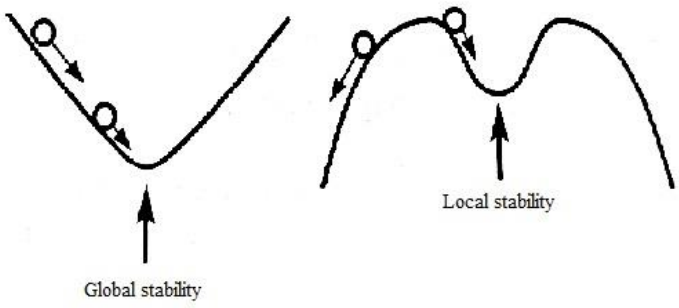

Figure 3.3 – Asymptotic stability concepts [14]

The above concepts of stability apply in general to nonlinear systems but can also apply to a particular case of linear systems, when described by the following equation.

$$\dot{x} = Ax \tag{3.6}$$

In the case of (3.6) the stability it is dependent on the position of the eigenvalues of A. Thus:

- If all the eigenvalues have negative real part, the origin of state space is asymptotically stable.
- If the linearized system has pure imaginary eigenvalues, nothing can be said about the nonlinear system.
- If it exists at least an eigenvalue on right side of semi plane (positive real part), the origin is unstable.
- If it exists non repeated eigenvalues over the imaginary axis, and all the others are in the negative real semi plane, the origin is stable, but not asymptotically stable.
- If it exists repeated eigenvalues over the imaginary axis, the origin is unstable.

The demonstration that if the eigenvalues have negative real part implies asymptotic stability is made using the Lyapunov direct method. This method will be discussed in the next section.

3.2 Lyapunov stability

Today Lyapunov stability is used in the control nonlinear systems. The name of Lyapunov is associated to the direct and indirect methods, but perhaps the principal method to control nonlinear systems is the direct method also called the second method of Lyapunov.

3.2.1 Direct method of Lyapunov

The second method of Lyapunov allows the demonstration of stability properties in an equilibrium point without using linearization, that is the reason for the name "direct", because this method uses the nonlinear equation directly. According to this method an equilibrium point is stable if it is possible to define a state function so called "Lyapunov function" in its neighbourhood [14].

3.2.2 Lyapunov functions

Before using the direct method of Lyapunov it is necessary to present some highlights about the state functions.

First, is necessary to consider a function V that transforms the state values $x \in \mathbb{R}^n$ in real numbers, and a scalar function $V(x): \mathbb{R}^n \to \mathbb{R}$. Assuming that V is continuous.

Assume V is continuous. In these conditions the function V is said to be positive definite in $\mathbb{R}^n$ if:

$$V(0) = 0$$
$$\forall_x \neq 0 : x \in \mathbb{R}^n \Rightarrow V(x) > 0 \tag{3.7}$$

V is said to be positive semi-definite in $\mathbb{R}^n$ if:

$$V(0) = 0$$
$$\forall_x \neq 0 : x \in \mathbb{R}^n \Rightarrow V(x) \geq 0 \tag{3.8}$$

V is said to be negative definite in $\mathbb{R}^n$ if:

$$V(0) = 0$$
$$\forall_x \neq 0 : x \in \mathbb{R}^n \Rightarrow V(x) < 0 \tag{3.9}$$

V is said to be negative semi-definite in $\mathbb{R}^n$ if:

$$V(0) = 0$$
$$\forall_x \neq 0 : x \in \mathbb{R}^n \Rightarrow V(x) \leq 0 \tag{3.10}$$

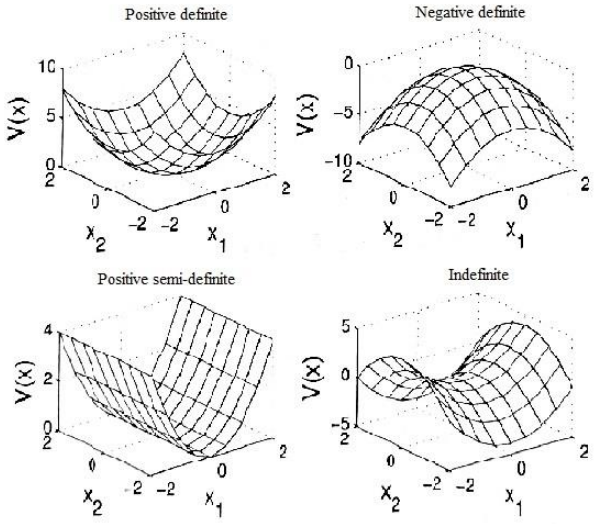

Figure 3.4 – State functions examples [14]

For a better understating, Fig. 3.4 illustrates graphically the state functions.

The function V relatively to (3.5) is said to be a "Lyapunov function" if its total derivate in order to time is negative semi-definite (3.11).

$$\frac{dV}{dt} \leq 0 \tag{3.11}$$

3.2.3 Simple Example of Lyapunov method

For better understanding of Lyapunov method, so called second method of Lyapunov, a very simple example will be presented.

Consider a system that can be represented by the following nonlinear state model:

$$\frac{dx_1}{dt} = -2x_1 - 2x_1{x_2}^2 \tag{3.12}$$

$$\frac{dx_2}{dt} = -2x_2 - 2x_2{x_1}^2 \tag{3.13}$$

The objective of this example is to show that the origin is asymptotically stable equilibrium point.

The origin is an equilibrium point $[0\ 0]^T$ because both derivates of the state are zero in that point.

To study system stability, the direct method of Lyapunov will be used. Start with considering the following candidate Lyapunov function.

$$V(x_1, x_2) = {x_1}^2 + {x_2}^2 \tag{3.14}$$

This function is continuous and its partial derivatives in order to x components are also continuous; the V function is also defined positive. The next step to study the stability using the second method of Lyapunov is to write the time derivative of (3.14):

$$\frac{dV}{dt} = 2x_1\frac{dx_1}{dt} + 2x_2\frac{dx_2}{dt} \tag{3.15}$$

Using (3.12) and (3.13) functions in (3.15):

$$\frac{dV}{dt} = -4({x_1}^2 + {x_2}^2 + 2{x_1}^2{x_2}^2) < 0 \tag{3.16}$$

$$\forall_{\begin{bmatrix} x_1 \\ x_2 \end{bmatrix}} \neq 0 \tag{3.17}$$

For all $x \neq 0$, by the local stability of Lyapunov theorem, the equilibrium point $[0\ 0]^T$ is asymptotically stable.

3.3 Sliding Mode Control

Sliding mode control (SMC) is a robust nonlinear stabilization technique used to control linear and nonlinear systems. SMC is characterized by two phases, sliding, and reaching [15]. The main idea of SMC is to use feedback controllers that operates in opposite sides of a "sliding manifold". The sliding manifold is independent of the model uncertainty, and it is designed in a way that the trajectories of the manifold converge to the equilibrium point [16]. The designed controller makes all the trajectories to converge towards the sliding manifold. When this region is reached, the system remains on it during the future times.

A simple example of the SMC technique will be present for a better understanding. Consider the closed-loop control application in the Fig. 3.5.

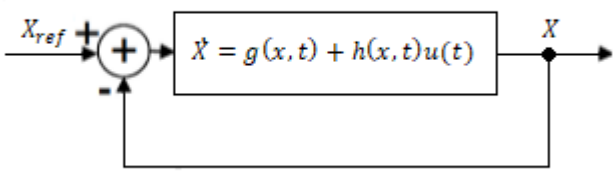

Figure 3.5 – Closed-loop control application

Where $x \epsilon \mathbb{R}^n$ is the state vector, $u \in \mathbb{R}$ is the control input, $g(x,t) \in \mathbb{R}^n$ and $h(x,t) \in \mathbb{R}^n$ are nonlinear functions. For this type of application it is better to consider a new state variable, the error (e) instead of the state variable x[17]. For this reason, consider the following equation:

$$e = X_{ref} - X \tag{3.18}$$

The purpose of this example is to force the error to tend to a neighbourhood of 0 using the SMC method. SMC used two phases, sliding, and reaching. In phase one it is needed to define a "sliding manifold".

Sliding manifold can be present as

$$s(x) = \left(k + \frac{dx}{dt}\right)^{n-1} e(x) \tag{3.19}$$

Through $s(x)$ the $e(x)$ will approach to 0, to maintain the system state bounded. From a geometric point of view $s(x) = 0$ defines the sliding manifold. The $s(x) = 0$ constructs a suitable manifold to slide while $e(x) \to 0$ as $t \to \infty$[15].

For simplicity reasons let's consider a first-order system n=2. The following equation is obtained from equation (3.19).

$$s(x) = ke(x) + \dot{e}(x) \tag{3.20}$$

In the second phase of the process the control input u should be able to enforce the system trajectories into the sliding manifold and achieve $s(x) = 0$ in finite time. To fulfil this phase, the direct method of Lyapunov will be use in the *s*-dynamics. For this reason, it is needed to have a candidate Lyapunov function, so let's consider the following candidate Lyapunov function in the *s*-dynamics.

$$V(s) = \frac{1}{2}s^2 \tag{3.21}$$

To guarantee the stability of the system the derivative of Lyapunov function must be negative definite. Therefore, the time derivative of (3.21) should satisfy the following condition.

$$\dot{V}(s) = s\dot{s} < 0 \tag{3.22}$$

The time derivative of the sliding manifold given in (3.20) is the following:

$$\dot{s} = k\dot{e} + \ddot{e} \tag{3.23}$$

The accomplishment of the inequality (3.22) guarantees the convergence of the system state trajectories to the sliding manifold $s(x) = 0$, if the control input u has the following form:

$$u = \begin{cases} 1 & if\ s(x) > 0 \wedge \dot{s}(x) > 0 \wedge u(t - \Delta t) = -1 \\ -1 & if\ s(x) < 0 \wedge \dot{s}(x) < 0 \wedge u(t - \Delta t) = 1 \end{cases} \tag{3.24}$$

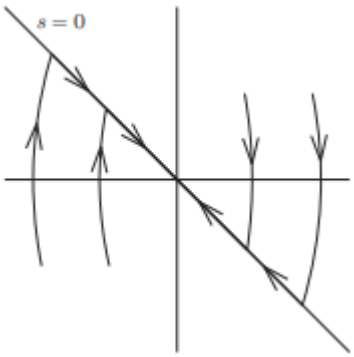

Figure 3.6 – Typical phase portrait (SMC) [16]

The Fig. 3.6 represents a Typical phase portrait of SMC.

The main disadvantage of SMC is the so called "chattering". Chattering appears because of switching control part, and this phenomenon is characterized by undesirable occurrence of oscillations with finite frequency and amplitude [15]. To overcome this problem in switching converters the input controller u on (3.24) must be substituted by a hysteresis comparator with a bandwidth of Δ. In this case the control input u will have the following form.

$$u = \begin{cases} 1 & if\ s(x) > \Delta \wedge \dot{s}(x) > 0 \wedge u(t - \Delta t) = -1 \\ -1 & if\ s(x) < -\Delta \wedge \dot{s}(x) < 0 \wedge u(t - \Delta t) = 1 \end{cases} \tag{3.25}$$

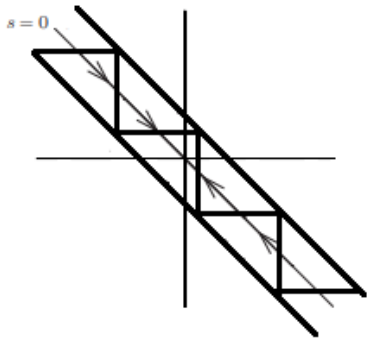

Figure 3.7 – Typical phase portrait (SMC) with a boundary layer Δ

The Fig. 3.7 represents a typical phase portrait with a boundary layer.

3.4 Backstepping Controller Design

Backstepping Controller design is a technique that is commonly used to control nonlinear systems with a triangular structure. The idea behind this method is to divide the problem in small problems (sub-problems), these sub-problems have a lower order system than the original problem. In order words the objective is to divide the complex problem into multiple and easier problems with lower order. It is possible to this because this procedure uses a few states as "virtual controls" to obtain the intermediate control laws with the control Lyapunov function (CLF) [18]. The advantages of backstepping control that was invented by Krstic, Kanellakopoulos, and Kokotovic are the assurance global of regional stability, the stress on robustness and computable transient performance [18]. This method is going to be used for the nonlinear system with the strict-feedback shape.

Consider the following nonlinear system with a strict-feedback form.

$$\begin{aligned} \dot{x}_1 &= f_1(x_1) + g_1(x_1)x_2 \\ \dot{x}_2 &= f_2(x_1, x_2) + g_2(x_1, x_2)x_3 \\ &\vdots \\ \dot{x}_n &= f_n(x_1, x_2, \dots, x_{n-1}, x_n) + g_n(x_1, x_2, \dots, x_{n-1}, x_n)u \end{aligned} \tag{3.26}$$

For the sake of simplicity let's consider a model of two cascades (3.27) and (3.28).

$$\dot{x}_1 = f_1(x_1) + g_1(x_1)x_2 \tag{3.27}$$

$$\dot{x}_2 = f_2(x_1, x_2) + g_2(x_1, x_2)u \tag{3.28}$$

Where, $x_1, x_2 \in \mathbb{R}^n$ are the state variables, $u \in \mathbb{R}^n$ is the control input, $f_1, g_1 \colon \mathbb{R}^n \to \mathbb{R}^n$, $f_2, g_2 \colon \mathbb{R}^n \times \mathbb{R}^n \to \mathbb{R}^{n \times n}$ are nonlinear functions.

To explain the basic backstepping design procedure consider the following example that uses (3.27) and (3.28). The objective of this example is to control (3.27) and (3.28) with backstepping control. It will be necessary two steps to solve de problem, the first one will consider just (3.27), and the second will consider the (3.27) and (3.28) together.

Step 1: The first thing to do is to find a suitable virtual control quantity. Consider the virtual control x_2, and denote it x_{2v}. Then, define a candidate Lyapunov function. The candidate Lyapunov function can be the following:

$$V_1 = \frac{1}{2}x_1^2 \tag{3.29}$$

The derivative of (3.29) must respect the (3.30) condition to be a "Lyapunov function"

$$\dot{V}_1 = x_1(f_1(x_1) + g_1(x_1)x_{2v}) \leq 0 \tag{3.30}$$

The algebraic control equation is given by (3.31)

$$f_1(x_1) + g_1(x_1)x_{2v} = c_1(x_1) \tag{3.31}$$

Where $c_1(x_1) = -C_1x_1$ and $C_1 > 0$. Then, it is possible to write the virtual control expression (3.32)

$$x_{2v} = g_1^{-1}(x_1)(-f_1(x_1) + c_1(x_1)) \tag{3.32}$$

Where $c_1(x_1)$ guarantees that $\dot{V}_1 < 0, x_1 \neq 0$ and the (3.32) solution is continuous.

Step 2: In this step the objective is to use (3.27) and (3.28). To do that a new candidate composite Lyapunov function is needed. The composite Lyapunov function is illustrated in (3.33)

$$V_2 = \frac{1}{2}x_1^2 + \frac{1}{2}(x_2 - x_{2v})^2 \tag{3.33}$$

As was made before the derivate of (3.33) must respect the (3.34) condition to be a "Lyapunov function"

$$\dot{V}_2 = x_1(f_1(x_1) + g_1(x_1)x_2) + (x_2 - x_{2v})(\dot{x}_2 - \dot{x}_{2v}) \leq 0 \tag{3.34}$$

The algebraic control equation is given by (3.35)

$$f_2(x_1, x_2) + g_2(x_1, x_2)u - \dot{x}_{2v} = -C_2(x_2 - x_{2v}) - g_1(x_1)x_1 \tag{3.35}$$

Where $c_2(x_1, x_2) = -C_2(x_2 - v_c) - g_1(x_1) + \dot{v}_c$ and $C_2 > 0$. Finally, it is possible to write the control expression (3.36)

$$u = {g_2}^{-1}(-f_2 + k_2(x_1, x_2)) \tag{3.36}$$

Where $c_2(x_1, x_2)$ guarantees that $\dot{V}_2 < 0, x_2 \neq x_{2v}$.

To sum up, the resulting control law u is asymptotically stable if $\dot{V}_2 < 0, \forall_{\begin{bmatrix} x_1 \\ x_2 \end{bmatrix}} \neq 0$.

Chapter 4

Nonlinear Controllers

The main objective of this chapter is to design nonlinear controllers that are able to control the DC voltage and current in the inverter-rectifier and in the DC-DC converter (figures 2.10 and 2.13).

Traditionally, controllers used to control voltage and current in power systems are linear and derived using linearized models pf the power network. Given the linear controllers simplicity and linear models, they are prone to fail under large deviations from the equilibrium point, around which the linearized models are obtained. Therefore, despite the increase in complexity, four nonlinear controllers are going to be designed, two of them to control voltage and current in the inverter-rectifier and the other two to control the similar quantities in the DC-DC converter. Hence, to do that the direct method of Lyapunov, backstepping, and sliding mode control are the techniques to be used.

Considering the four-terminal HVDC line, and the interconnection DC line (Fig.2.1), to control de grid DC voltage the control strategy considers a voltage controller in thee inverter-rectifier of line 1, while in line 3 a direct power injection is assumed in the line 3 inverter-rectifier. In this way is it possible to control the grid voltage and the power dispatched in the network. Therefore, in this chapter it will be explained the design of power and voltage controllers.

4.1 Inverter-rectifier Controllers

Some techniques to design nonlinear controllers for voltage and current control have been introduced in chapter 3. Therefore, backstepping will be used to control the line voltage [19], while current controllers are based on sliding mode control, discussed in section 3.3. To control the power to be injected in line 3 (figure 2.1), a power controller in dq coordinates will be introduced based on a sliding mode controller.

4.1.1 Nonlinear Voltage Controller of the DC-AC Converter

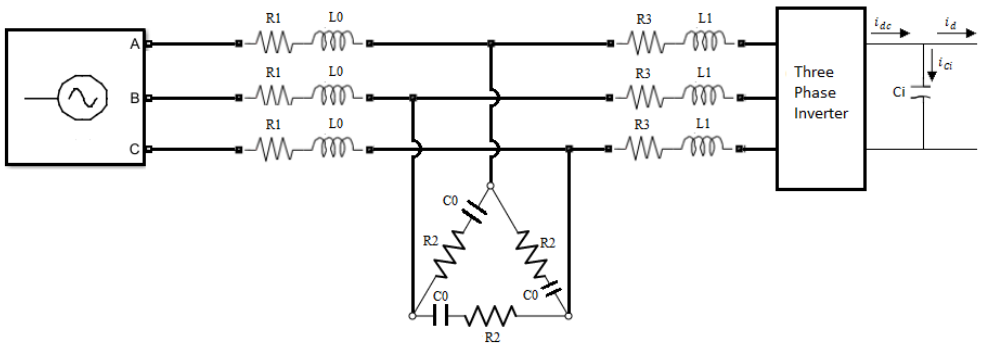

Figure 4.1 - Output inverter currents representation

Considering the Fig. 4.1 the system model in d-q coordinates is expressed as follows:

$$\frac{du_{Ci}}{dt} = \frac{1}{C_i}\left(\frac{u_{Gi}}{u_{Ci}} i_d + i_{dc}\right) = \frac{1}{C_i}(G_i i_d + i_{dc})$$
$$\frac{di_d}{dt} = \frac{-G_i u_{Ci} - R_3 i_d + u_{Gi}}{L_1} + \omega i_q \qquad (4.1)$$

The virtual control input is the inverter-rectifier input current d component $G_i i_d$, where $G_i = \frac{u_{Gi}}{u_{Ci}}$ is the current gain.

The control objective is defined as $u_{Ci} = u_{Ciref}$, to obtain the control law $G_i u_{Ci} = f(u_{Ciref}, u_{Ci})$.

Considering a new variable e_u, the control objective error, defined as:

$$e_u = u_{Ciref} - u_{Ci} \tag{4.2}$$

The purpose is to demand $e_u = 0$. To present steady-state errors add an integral of the objective error by defining:

$$e_I = \int_0^t e_u dt = 0 \tag{4.3}$$

According to Lyapunov the system is asymptotically stable if the candidate Lyapunov function verifies the following conditions:

$$\begin{aligned} &V(x = 0) = 0 \\ &V(x \neq 0) > 0 \\ &V(|x| \to \infty) \to \infty \\ &\dot{V}(x \neq 0) < 0 \end{aligned} \tag{4.4}$$

Therefore, the stability condition is defined as:

$$V(x \neq 0)\dot{V}(x \neq 0) < 0 \tag{4.5}$$

Hence, it is necessary to define a positive definite candidate Lyapunov function (4.6).

$$V = k_I \frac{{e_I}^2}{2} + \frac{{e_u}^2}{2} \tag{4.6}$$

According to direct method of Lyapunov (discussed in the previous chapter), the time derivative of V must be negative. To guarantee that this condition is verified the virtual input current must obey $i_d = i_{dv}$ for $k_u > 0, \Rightarrow k_I > 0$.

$$\frac{dV}{dt} < 0 \;\Rightarrow\; k_I e_I \frac{de_I}{dt} + e_u \frac{de_u}{dt} = -k_u {e_u}^2 \tag{4.7}$$

From the (4.7):

$$k_I e_I e_u + e_u \left(\frac{du_{Ciref}}{dt} - \frac{du_{Ci}}{dt} \right) = -k_u {e_u}^2 \tag{4.8}$$

Providing:

$$k_I e_I + \left(\frac{du_{Ciref}}{dt} - \left(\frac{G_i}{C_i} i_{dv} + \frac{i_{dc}}{C_i} \right) \right) = -k_u e_u \tag{4.9}$$

Therefore, the virtual control action is the following:

$$i_{dv} = \frac{u_{Ci}}{u_{Gi}} \left(C_i \left(k_I e_I + k_u e_u + \frac{du_{Ciref}}{dt} \right) - i_{dc} \right) \tag{4.10}$$

Equation (4.10) is the Lyapunov equivalent of a PI controller, since the virtual control action i_{dv} depends on the e_u and on the integral e_I of the error e_u.

Fig. 4.2 presents the block diagram of the nonlinear voltage controller in the inverter-rectifier.

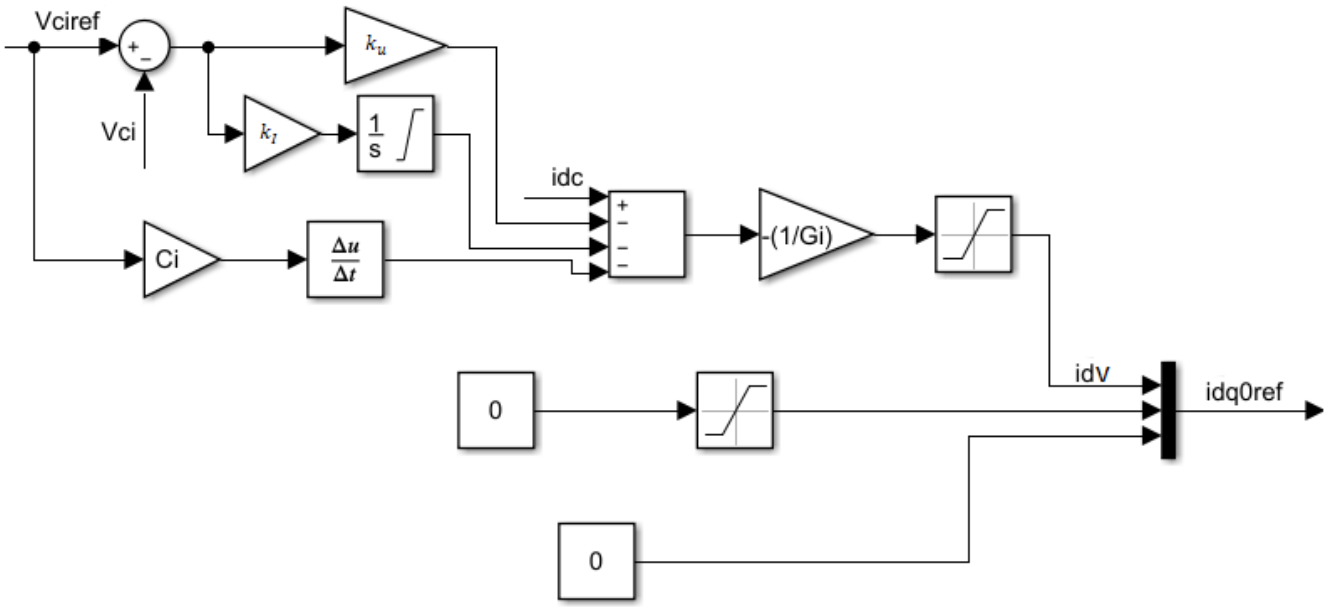

Figure 4.2 – Nonlinear voltage controller of the inverter-rectifier representation

From (4.10) a nonlinear voltage controller is obtained. This controller will generate a i_{dq0ref} that will be used in the nonlinear current controller. However, the nonlinear current controller will work in $\alpha\beta$ coordinates hence, the i_{dq0ref} will be transformed in $i_{\alpha\beta}$ through the following transformation matrix [20]:

$$\begin{bmatrix} i_\alpha \\ i_\beta \\ i_0 \end{bmatrix} = \begin{bmatrix} \cos(\omega t) & -\sin(\omega t) & 0 \\ \sin(\omega t) & \cos(\omega t) & 0 \\ 0 & 0 & 1 \end{bmatrix} \begin{bmatrix} i_d \\ i_q \\ i_0 \end{bmatrix} \tag{4.11}$$

The V_{ciref} present in the figure 4.2 is express as follows:

$$V_{ciref} = V_n - R_e P \tag{4.12}$$

Where R_e represents the droop control factor. In this case the droop control is characterized by a voltage variation rate with the active power transmitted. The R_e units will be Volt per Watt.

The droop control is present in Fig. 4.3.

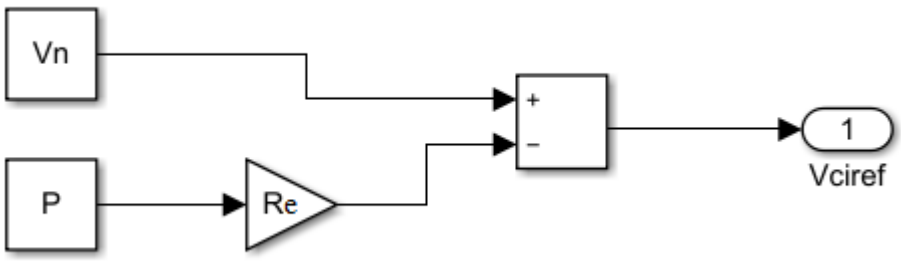

Figure 4.3 – Droop control representation

4.1.2 Power Controller

For the sake of simplicity, the power controller will be design in dq coordinates. Hence, the measure voltage in abc coordinates will be transformed in dq coordinates by the transformation matrix present in (4.13) [20]. Thereby,

it is possible to have a simpler control system, once instead of the three time-dependent signs the system will be composed by two continuous signals (V_d, V_q).

$$\begin{bmatrix} V_d \\ V_q \\ V_0 \end{bmatrix} = \sqrt{\frac{2}{3}} \begin{bmatrix} \cos \omega t & \cos\left(\omega t - \frac{2\pi}{3}\right) & \cos\left(\omega t - \frac{4\pi}{3}\right) \\ -\sin \omega t & -\sin\left(\omega t - \frac{2\pi}{3}\right) & -\sin\left(\omega t - \frac{2\pi}{3}\right) \\ \frac{1}{\sqrt{2}} & \frac{1}{\sqrt{2}} & \frac{1}{\sqrt{2}} \end{bmatrix} \begin{bmatrix} V_a \\ V_b \\ V_c \end{bmatrix} \tag{4.13}$$

Therefore, the active and reactive power in dq coordinates can be calculated as follows [21]:

$$\begin{cases} P = v_d i_d + v_q i_q \\ Q = v_q i_d - v_d i_q \end{cases} \tag{4.14}$$

After some mathematical manipulation, equation (4.14) can be solved for i_d, i_q, giving (4.15).

$$\begin{cases} i_d = \dfrac{P v_d + Q v_q}{{v_d}^2 + {v_q}^2} \\ i_q = \dfrac{P v_q - Q v_d}{{v_d}^2 + {v_q}^2} \end{cases} \tag{4.15}$$

The i_{dq} present in (4.15) will be used in the nonlinear current controller but in α, β coordinates, trough the transformation matrix (4.11).

4.1.3 Nonlinear Current Controller of the DC-AC Converter

Considering the Fig. 2.10, the AC currents dynamics is (4.16).

$$L \frac{di_k}{dt} = V_{kN} - R i_K - e_k \; ; k \in \{A, B, C\} \tag{4.16}$$

Using α, β transformation, and denoting $i_{\alpha,\beta}$ for to represent both i_α, and i_β, it is possible to rewrite (4.16) as follows:

$$L \frac{di_{\alpha,\beta}}{dt} = V_{\alpha,\beta} - R i_{\alpha,\beta} - e_{\alpha.\beta} \tag{4.17}$$

Using sliding mode control, the control objective can be defined in the following equation:

$$e_{i_{\alpha,\beta}} = i_{\alpha,\beta v} - i_{\alpha,\beta} = 0 \tag{4.18}$$

Therefore, the time-varying linear surface $s(x)$ is defined as:

$$s(x) = i_{\alpha,\beta v} - i_{\alpha,\beta} = e_{i_{\alpha,\beta}} \tag{4.19}$$

To enforce the sliding surface reaching after a finite time it is needed the use of the second method of Lyapunov as a stability condition. Hence, the candidate Lyapunov function can be express as:

$$V = \frac{1}{2} s^2 = \frac{{e_{i_{\alpha,\beta}}}^2}{2} \tag{4.20}$$

The stability condition according to Lyapunov is given by:

$$e_{i_{\alpha,\beta}} \frac{de_{i_{\alpha,\beta}}}{dt} < 0 \tag{4.21}$$

Thus, the control conditions can be express by:

$$\begin{cases} If\ e_{i_{\alpha,\beta}} > 0 \Rightarrow i_{\alpha,\beta} \uparrow \Rightarrow V_{\alpha,\beta} > R i_{\alpha,\beta} + e_{\alpha,\beta} \\ If\ e_{i_{\alpha,\beta}} < 0 \Rightarrow i_{\alpha,\beta} \downarrow \Rightarrow V_{\alpha,\beta} < R i_{\alpha,\beta} + e_{\alpha,\beta} \end{cases} \tag{4.22}$$

Where,

$$i_{\alpha,\beta} = i_{\alpha,\beta v} \pm \Delta i/2 \qquad (4.23)$$
$$i_{\alpha,\beta} \in [i_{\alpha,\beta v} - \Delta i/2\,, i_{\alpha,\beta v} + \Delta i/2]$$

Considering (4.22) the reaching condition is given by:

$$V_{\alpha,\beta} > \left| R i_{\alpha,\beta} + e_{\alpha.\beta} \right| \qquad (4.24)$$

The objective of this control is to achieve a zero error between the reference value and the variables to control. This would imply an infinite switching frequency which is not possible, because the semiconductors have physical speed limitations. Hence, to circumvent this issue the error must be bounded. Therefore, the nonlinear current control based on sliding mode control theory will be given by the following conditions:

$$\begin{cases} If\ e_{i_{\alpha,\beta}} > +\dfrac{\Delta i}{2} \Rightarrow \delta_{\alpha,\beta} = 1 \Rightarrow i_{\alpha,\beta v} > i_{\alpha,\beta} \Rightarrow i_{\alpha,\beta} \uparrow \Rightarrow \dfrac{di_{\alpha,\beta}}{dt} > 0 \Rightarrow V_{\alpha,\beta} > 0 \\ If\ -\dfrac{\Delta i}{2} < e_{i_{\alpha,\beta}} < +\dfrac{\Delta i}{2} \Rightarrow \delta_{\alpha,\beta} = 0 \Rightarrow i_{\alpha,\beta v} \approx i_{\alpha,\beta} \Rightarrow i_{\alpha,\beta} \uparrow\downarrow \Rightarrow \dfrac{di_{\alpha,\beta}}{dt} \approx 0 \Rightarrow V_{\alpha,\beta} = 0 \\ If\ e_{i_{\alpha,\beta}} < -\dfrac{\Delta i}{2} \Rightarrow \delta_{\alpha,\beta} = -1 \Rightarrow i_{\alpha,\beta v} < i_{\alpha,\beta} \Rightarrow i_{\alpha,\beta} \downarrow \Rightarrow \dfrac{di_{\alpha,\beta}}{dt} < 0 \Rightarrow V_{\alpha,\beta} < 0 \end{cases} \qquad (4.25)$$

Considering the conditions present in (4.25) the following table 4.1 can be obtained:

Table 4.1 – Vector selection table

		$e_{i\alpha}$		
		$\delta_\alpha = -1$	$\delta_\alpha = 0$	$\delta_\alpha = 1$
$e_{i\beta}$	$\delta_\beta = 1$	3	2 or 3	2
	$\delta_\beta = 0$	4	0 or 7	1
	$\delta_\beta = -1$	5	5 or 6	6

The nonlinear current controller of the inverter-rectifier will be composed by three-level comparators and a table of truth that are responsible for all possible combinations of the vectors as it possible to see in Fig. 4.4.

The table of truth present in Fig.4.4 was build considering the table 4.1.

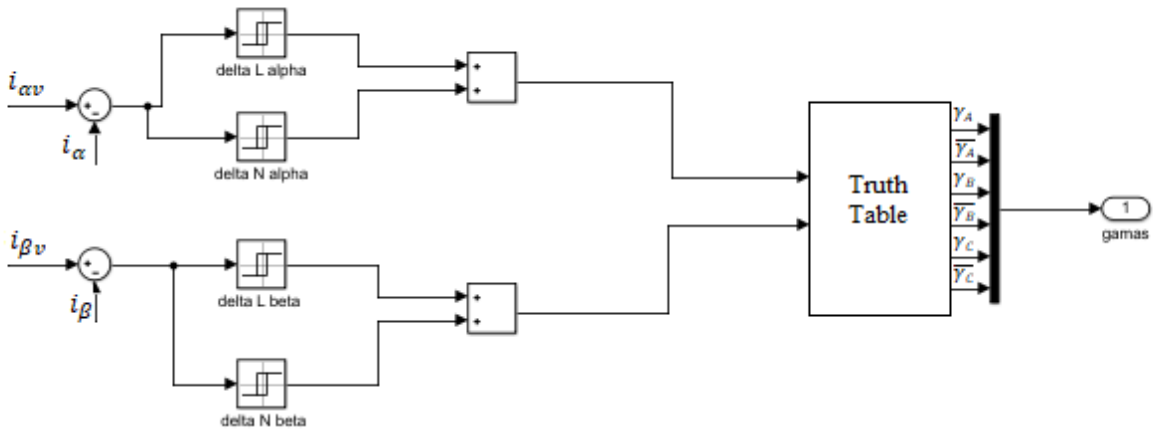

Figure 4.4 – Nonlinear current controller of the inverter representation

The i_α and i_β will provided by the i_{abc} currents (Fig.4.4) transformed in to $\alpha\beta 0$ coordinates trough the following transformation matrix [20]:

$$\begin{bmatrix} i_\alpha \\ i_\beta \\ i_0 \end{bmatrix} = \begin{bmatrix} 1 & -\frac{1}{2} & -\frac{1}{2} \\ 0 & \frac{\sqrt{3}}{2} & -\frac{\sqrt{3}}{2} \\ \frac{1}{\sqrt{2}} & \frac{1}{\sqrt{2}} & \frac{1}{\sqrt{2}} \end{bmatrix} \begin{bmatrix} i_a \\ i_b \\ i_c \end{bmatrix} \tag{4.26}$$

4.2 DC-DC Converter Controllers

As said the multiterminal DC network contains constant power and constant current electronic loads. These electronic loads will be simulated using three-level DC-DC converters. To control current and voltage in the DC-DC converters similar nonlinear controllers used earlier (sections 3.3 and 3.4) will be applied. Therefore, in this section the combination between backstepping and sliding mode control will be the chosen method. First, the backstepping method is used to control voltage by defining a virtual control current, while a sliding mode current controller will be used to enforce the DC current to track the virtual current reference.

4.2.1 Nonlinear Voltage Controller of the DC-DC Converter

Appling the same principle of section 4.1.1, considering Fig. 2.13 the dynamic behaviour of the DC currents is the following:

$$\begin{cases} \frac{dv_c}{dt} = \frac{i_L - i_0}{C} \\ \frac{di_L}{dt} = \frac{V_i - V_0}{L} \end{cases} \tag{4.27}$$

In this case the control objective is defined as:

$$V_0 = V_{0ref} \tag{4.28}$$

Moreover, the error (e_{v_0}) between the reference voltage and the capacitor voltage is express as:

$$e_{V_0} = V_{0ref} - V_0 \tag{4.29}$$

The candidate Lyapunov function is defined as:

$$V_L = \frac{{e_{V_0}}^2}{2} \tag{4.30}$$

The Lyapunov function (4.30) must verified the (4.4) and (4.5) conditions to be asymptotically stable. Therefore, $V_L > 0 \; \forall e_{V_0} \neq 0$ and $V_L \to \infty \; for \; \|t\| \to \infty$.

The candidate Lyapunov function time derivative must be a negative definite as was explained before (4.31).

$$\dot{V}_L = e_{V_0} \frac{de_{V_0}}{dt} = -K_V {e_{V_0}}^2 \quad , K_V > 0 \tag{4.31}$$

According to the second method of Lyapunov the global asymptotic stability is defined as:

$$\frac{de_{V_0}}{dt} = -K_V e_{V_0} \Rightarrow \frac{de_{V_0}}{dt} = \frac{de_{V_{0ref}}}{dt} - \frac{i_L - i_0}{C} \tag{4.32}$$

Where, $e_{V_0} \neq 0$, the $\frac{de_{V_0}}{dt}$ using (4.27) and (4.29) is defined as:

$$\frac{de_{V_0}}{dt} = -K_V e_{V_0} \Rightarrow \frac{de_{V_0}}{dt} = \frac{de_{V_{0ref}}}{dt} - \frac{i_L - i_0}{C} \tag{4.33}$$

Thus, replacing in the previous equation (4.33) i_L by i_{Lref} where, i_{Lref} is the virtual control variable, it is possible to control V_0 by defining i_{Lref}:

$$\frac{de_{V_{0ref}}}{dt} - \frac{i_{Lref} - i_0}{C} = -K_V e_{V_0} \Rightarrow i_{Lref} = CK_V e_{V_0} + C\frac{de_{V_{0ref}}}{dt} + i_0 \tag{4.34}$$

Hence, the nonlinear voltage controller will be represented by the Fig. 4.5.

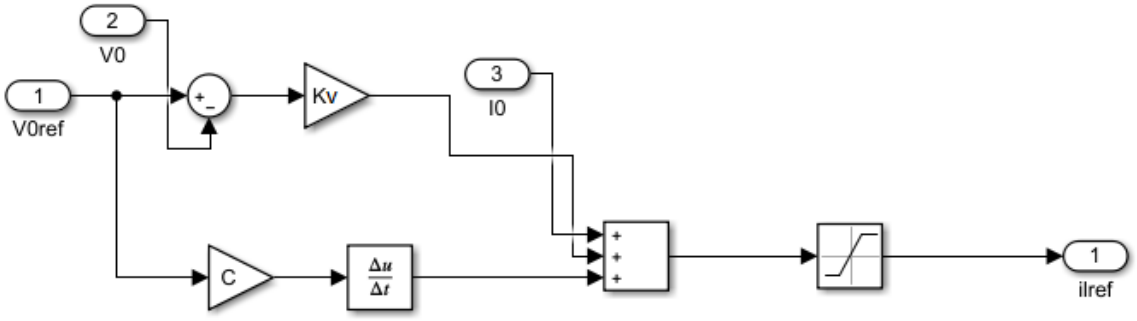

Figure 4.5 – Nonlinear voltage controller Simulink representation of the DC-DC converter

4.2.2 Nonlinear Current Controller of the DC-DC Converter

To design the nonlinear current controller the same principle of section 4.1.2 will be applied, but in this case to a DC-DC converter [12].

Considering the Fig. 2.13 is possible to write the following dynamic equation:

$$L\frac{di_L}{dt} = V_i - V_0 \tag{4.35}$$

Considering equation (2.43) it is possible to rewrite equation (4.35) as follows:

$$\frac{di_L}{dt} = \frac{\gamma U - V_0}{L} \tag{4.36}$$

The control objective is given by the following equation:

$$e_{i_L} = i_{Lref} - i_L = 0 \tag{4.37}$$

Moreover, the time-varying linear surface $s(x)$ is defined as:

$$s(x) = i_{Lref} - i_L = e_{i_L} \tag{4.38}$$

To enforce that the sliding surface is reached after a finite period is needed the use of the second method of Lyapunov as a stability condition. Therefore, the candidate Lyapunov function can be express as:

$$V = \frac{1}{2}s^2 = \frac{{e_{i_L}}^2}{2} \tag{4.39}$$

The stability condition according to the direct method of Lyapunov is satisfied, if $s\dot{s} < 0$. Thus:

$$\begin{aligned} &If, e_{i_L} > \frac{\Delta i_L}{2} \Rightarrow i_L \uparrow \Rightarrow \gamma = 1 \quad If, \gamma U > V_0 \\ &If, -\frac{\Delta i_L}{2} < e_{i_L} < \frac{\Delta i_L}{2} \Rightarrow \gamma = 0 \\ &If, e_{i_L} < -\frac{\Delta i_L}{2} \Rightarrow i_L \downarrow \Rightarrow \gamma = -1 \end{aligned} \tag{4.40}$$

Therefore, the nonlinear current controller will be represented by the Fig. 4.5.

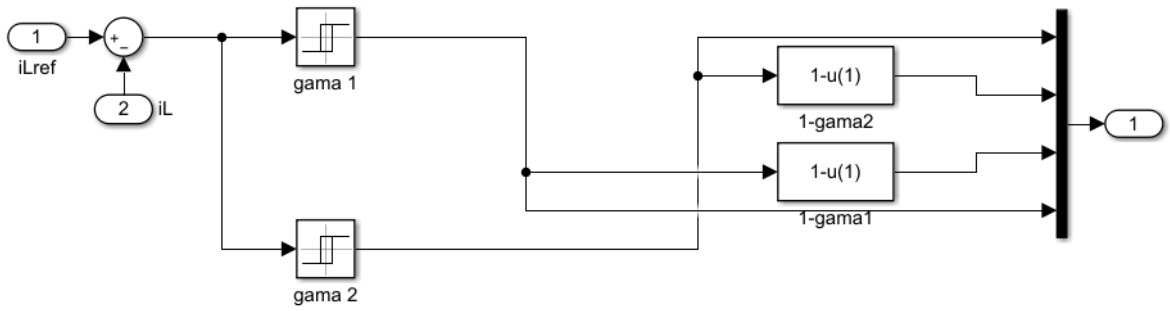

Figure 4.6 – Nonlinear current controller Simulink representation of the DC-DC converter

As it can be seen in figure 4.5, the nonlinear current controller has a decoder that as the following truth table:

Table 4.2 – Truth Table of the figure 4.4

γ_1	γ_2	S_1	S_2	S_3	S_4
0	0	0	1	1	0
0	1	1	0	1	0
1	1	1	0	0	1
1	0	0	1	0	1

Therefore, the driving signals S_1 to S_4 of the DC-DC converter (Fig. 2.13) are obtained from table 4.2 as follows:

$$\begin{aligned} S_1 &= \gamma_2 \\ S_4 &= \gamma_1 \\ S_2 &= \overline{S_1} = \overline{\gamma_2} \\ S_3 &= \overline{S_4} = \overline{\gamma_1} \end{aligned} \tag{4.41}$$

In the next chapter PI controllers are going to be designed to serve as the reference comparisons for the nonlinear controllers.

Chapter 5

Multiterminal Network Linear Control

In this chapter the main objective is to design linear controllers like Proportional-Integral (PI), to control the DC line voltage and the load currents. PI controllers are commonly used in power systems especially in voltage-sourced converter devices. This type of controllers is used in this application because it presents a simple structure, good overall dynamic behaviour and is intuitive to design [22]. Therefore, a PI voltage controller will be designed for the inverter-rectifier while voltage and current PI controllers will be designed for the DC-DC converters.

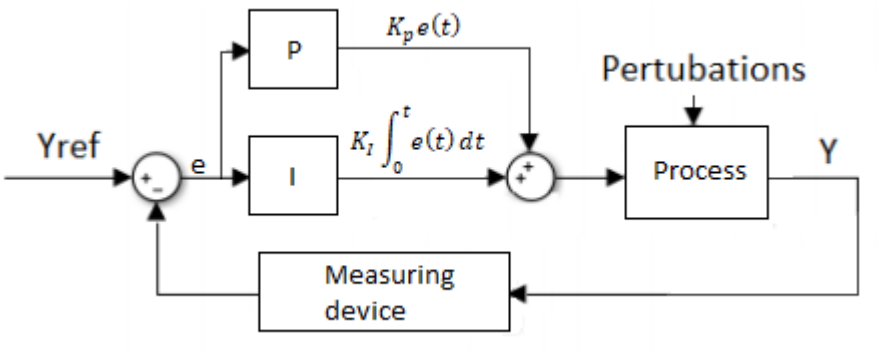

Figure 5.1 – Closed loop block diagram of a PI controller modified from [23]

The PI controller (Fig. 5.1) is enclosed in a closed loop system with feedback. The PI computes the tracking error, the difference between the reference value and the measure value. Then, the error is processed by the proportional (P) and integral (I) blocks. The P term is proportional to the error. In the other hand, the I term integrates over time the error to generate the integral of past errors. When zero tracking error is reached the I term becomes constant. The I term is responsible to guarantee zero steady state error, even when disturbances occur. The P term helps to improve the speed of the system [23]. Therefore, the combination of P and I terms is crucial to perform as required.

The PI transfer function of the Fig. 5.1 can be defined as follows:

$$v(t) = K_p e(t) + K_I \int_0^t e(t)dt \tag{5.1}$$

Where, K_p is the proportional gain and K_I is the integral gain. Usually these gains are constant and have moderate to low values depending on the system closed loop dynamics. As usually some high frequency poles are neglected, if K_p or K_I are too big the system can become unstable or strongly overshoot the reference value. If K_I is too small, the output will slowly converge to the reference.

The transfer function of (5.1) in Laplace domain is defined as:

$$K(s) = K_p + \frac{K_I}{s} \tag{5.2}$$

The closed loop transfer function in Laplace domain of the block diagram in Fig. 5.1 can be express as follows, supposing unity feedback gain:

$$G(s) = \frac{K(s)H(s)}{1 + K(s)H(s)} \tag{5.3}$$

Where, $K(s)$ is the PI transfer function and $H(s)$ is the plant transfer function. If $K(s)H(s) = -1$ the system is said unstable, if the term in denominator $K(s)H(s)$ is smaller than 1, the stability is guaranteed [23].

The Fig. 5.2 represents the adjustments of the proportional and integral terms to produce the best results in the case of voltage regulation.

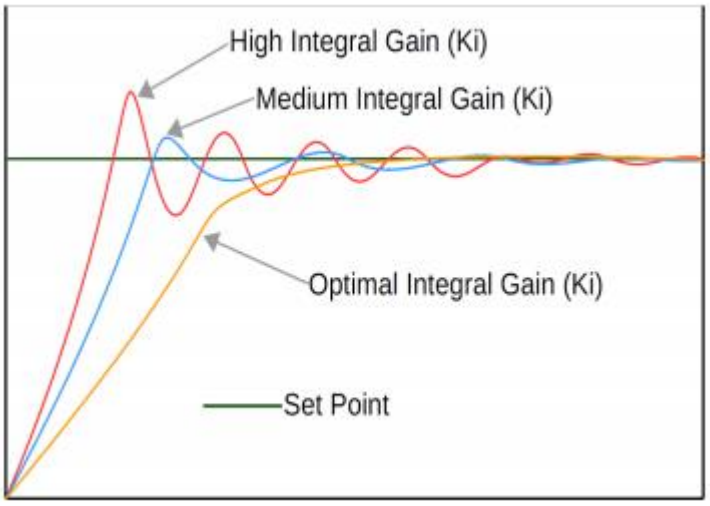

Figure 5.2 – Step response with different coefficients [23]

5.1 Linear Voltage Controller of the Inverter-Rectifier

To design the linear voltage controller the PI method is going to be the chosen [21]. From a simpler point of view, the controller will be design in dq coordinates instead of abc coordinates because dq is a continuous state and abc is time dependent.

Considering the Fig. 2.10 the equations of the current dynamics in dq coordinates is express as follows:

$$\begin{cases} u_d = L\dfrac{di_d}{dt} + Ri_d - \omega L i_q + e_d \\ u_q = L\dfrac{di_q}{dt} + Ri_q + \omega L i_d + e_q \end{cases} \tag{5.4}$$

The active and reactive power in the connection to the three-phase source are defined as:

$$\begin{cases} P_d = e_d i_d \\ P_q = -e_d i_q \end{cases} \tag{5.5}$$

The current i_{dc} defined in the Fig. 4.1 is expressed as:

$$i_{dc} = i_d + i_{ci} \tag{5.6}$$

Considering a reference frame with $e_q = 0$, the active and reactive power in the connection to the three-phase source are defined as:

$$P_d = e_d i_d = V_n i_{dc} \Rightarrow i_{dc} = \frac{e_d}{V_n} i_d \Rightarrow i_{dc} = G_i i_d \tag{5.7}$$

Where, $G_i = \frac{e_d}{V_n}$, and $e_d = \sqrt{2}\frac{V_{nac}}{\sqrt{3}}$.

The dynamic equation of DC voltage is the following:

$$C_i \frac{dv_{ci}}{dt} = i_{dc} - i_d \tag{5.8}$$

The nonlinear sliding mode current controller (section 4.1.3) is here approximated by the transfer function:

$$\frac{i_{dc}}{i_{dref}} = \frac{G_i/\alpha_i}{T_{dv}s + 1} \tag{5.9}$$

Where, α_i is the current sensor gain, T_{dv} is the average delay time of the i_d current relatively to its reference value i_{dref}. The G_i/α_i is caracterized by a gain while $T_{dv}s + 1$ is the dominant pole (high frequency poles are neglected).

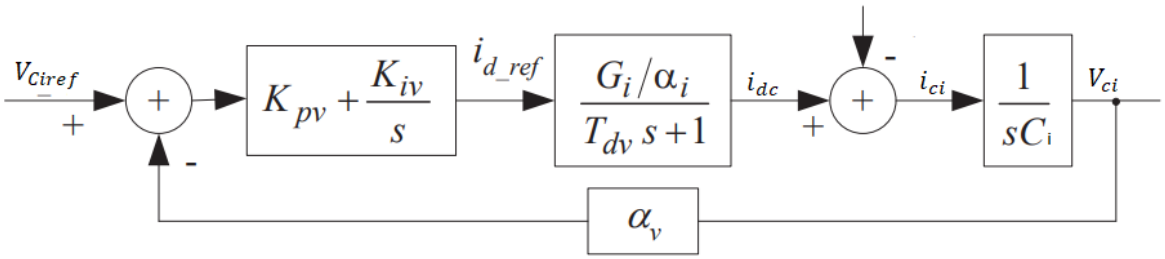

Figure 5.3 – Closed loop block diagram of voltage modified from [21]

Considering Fig. 5.3 the closed loop transferer function is express as:

$$\frac{V_{ci}}{V_{ciref}} = \frac{\frac{\alpha_v G_i}{\alpha_i}\frac{K_{pv} + sK_{iv}}{T_{dv}C_i}}{s^3 + s^2\frac{1}{T_{dv}} + s\frac{\alpha_v G_i K_{pv}}{\alpha_i T_{dv} C_i} + \frac{\alpha_v G_i K_{iv}}{\alpha_i T_{dv} C_i}} \tag{5.10}$$

Where, T_{dv} is the time delay, α_i is the current sensor gain, α_v is the voltage sensor gain, K_{iv} is the integral gain and K_{pv} is the proportional gain.

Considering the ITAE criteria the proportional and integral gains are defined as follows [23]:

$$K_{pv} = \frac{2.15 C_i \alpha_i}{1.75^2 \alpha_v G_i T_{dv}}$$
$$K_{iv} = \frac{C_i \alpha_i}{1.75^3 \alpha_v G_i {T_{dv}}^2} \tag{5.11}$$

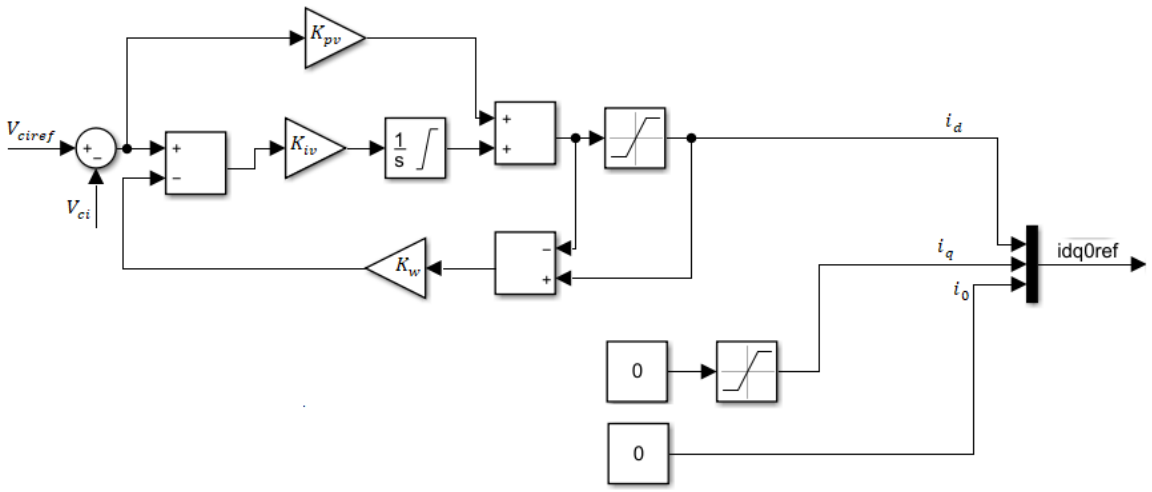

Figure 5.4 – Linear voltage controller of the inverter representation

The K_w present in Fig. 5.4 represents the anti-windup gain for big signal variations. An anti- windup system results in less overshoots in voltage and lower control effort. The omission of this gain can cause a considerable deterioration of the response.

The anti-windup gain is defined as:

$$K_w = -K_{iv} \tag{5.12}$$

The controller present in Fig. 5.4 will generate a i_{dq0ref} that will be used in the nonlinear current controller (section 4.1.3) here represented by the transfer function (5.9)

5.2 Linear Controller of the DC-DC Converter

In this section two linear PI controllers will be designed for the DC-DC converter to control current and voltage.

5.2.1 Linear Current Controller of the DC-DC Converter

From the Fig. 2.13 assuming that the control current is i_L ($i_L = i_{Lref}$).

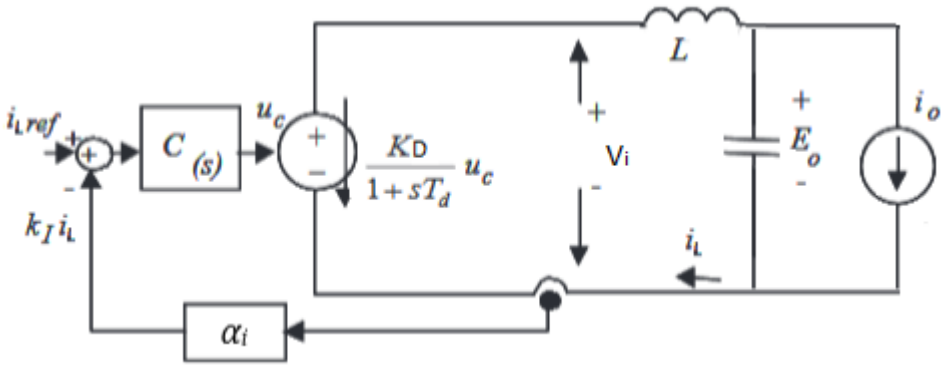

Figure 5.5 – Equivalent diagram of linear current control modified from [12]

From Fig. 5.5 applying the Kirchhoff laws the following equation in the Laplace domain is obtained:

$$i_L(s) = \frac{V_i - E_0}{sL} \tag{5.13}$$

The block diagram C(s), (figure 5.5), of the linear current controller is represented in the figure 5.6.

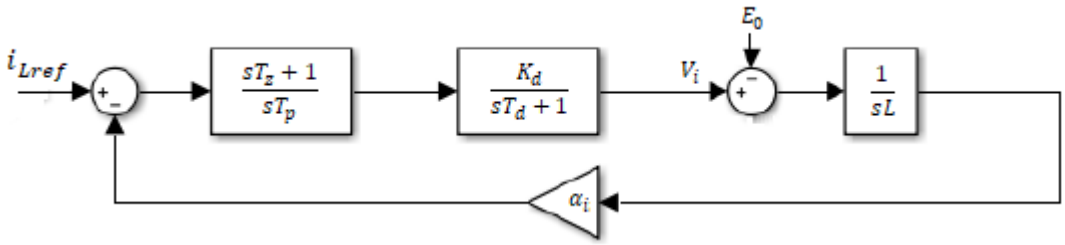

Figure 5.6 – Block diagram of linear current control

A PI controller is used to eliminate static error as the disturbance E_0 is in the input of the plant integrator. The closed loop transfer function of Fig. 5.6 is given by:

$$i_L(s) = \frac{(1+sT_z)i_{L\,ref}(s) - \frac{sT_p(1+sT_d)}{K_d\alpha_i}E_0(s)}{s^3\frac{LT_dT_p}{K_d\alpha_i} + s^2\frac{LT_p}{K_d\alpha_i} + sT_z + 1} \tag{5.14}$$

The criteria $b_{k^2} = a_i b_{k-1} b_{k+1}$ ensuring stability is applied to the terms of the denominator of (5.14) so that the values of T_p and T_z can be obtained [12].

$$\begin{cases} {T_z}^2 = a_i \dfrac{LT_p}{k_d \alpha_i} \\ \left(\dfrac{LT_p}{K_d \alpha_i}\right)^2 = a_i T_z \dfrac{LT_p T_d}{K_d \alpha_i} \end{cases} \Rightarrow \begin{cases} T_z = {a_i}^2 T_d \\ T_p = \dfrac{{a_i}^3 {T_d}^2 K_d \alpha_i}{L} \end{cases} \tag{5.15}$$

Where $\alpha_i = 3$, to have small overshoot at the expense of a slower response.

Substituting T_z and T_p in the (5.14) closed loop transfer function:

$$\frac{i_L(s)}{i_{Lref}(s)} = \frac{(1 + {a_i}^3 T_d s)}{{a_i}^3 {T_d}^3 s^3 + {a_i}^3 {T_d}^2 s^2 + {a_i}^2 T_d s + 1} \tag{5.16}$$

The K_{pi} and K_{ii} gains are given by:

$$\begin{cases} K_{pi} = \dfrac{T_z}{T_p} \\ K_{ii} = \dfrac{1}{T_p} \end{cases} \tag{5.17}$$

The linear current controller to the DC-DC converter can be represented in the Fig. 5.7.

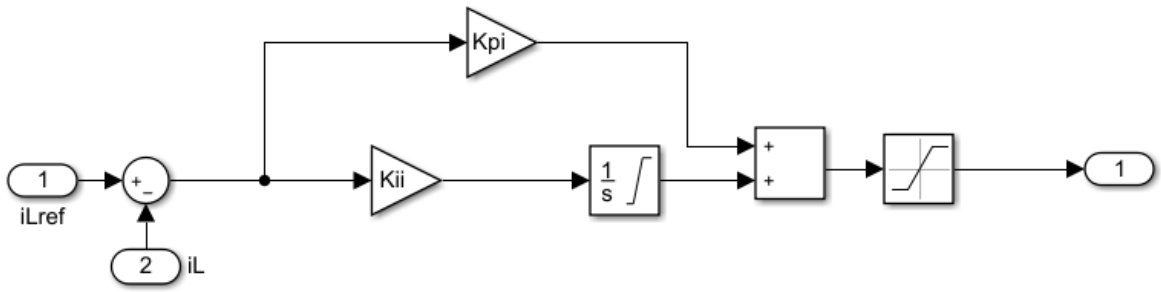

Figure 5.7 – Linear current controller of the DC-DC converter representation

5.2.2 Linear Voltage Controller of the DC-DC Converter

The objective is to control the voltage in DC-DC converter present in figure 2.13. Therefore, from the Fig. 5.5 to control the output voltage E_0 ($E_0 = E_{0ref}$) is necessary to consider the block diagram in the Fig. 5.8.

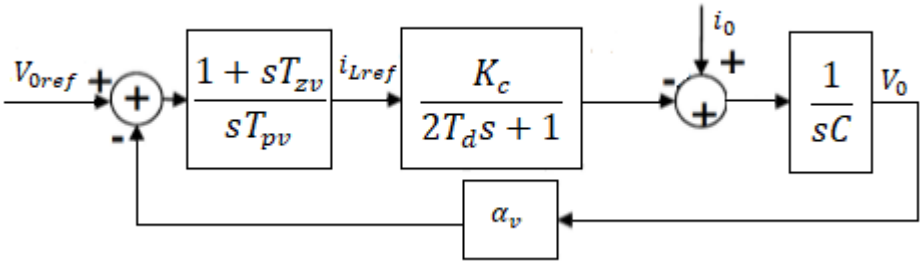

Figure 5.8 – Block diagram of linear voltage control modified from [12]

The closed loop transfer function of figure 5.8 is:

$$V_0(s) = \frac{\frac{1+sT_{zv}}{sT_{pv}} \frac{K_c}{2T_d s+1} \frac{1}{sC}}{1+\frac{1+sT_{zv}}{sT_{pv}} \frac{K_c}{2T_d s+1} \frac{1}{sC} \alpha_v} V_{0ref}(s) + \frac{\frac{1}{sC}}{1+\frac{1+sT_{zv}}{sT_{pv}} \frac{K_c}{2T_d s+1} \frac{1}{sC} \alpha_v} i_0(s)$$

$$\Leftrightarrow V_0(s) = \frac{K_c(1+sT_{zv})}{s^2T_{pv}C(2T_ds+1)+K_c\alpha_v(1+sT_{zv})}V_{0ref}(s) + \frac{sT_{pv}(2T_ds+1)}{2s^3T_dT_{pv}C+s^2T_{pv}C+sT_{zv}K_c\alpha_v+K_c\alpha_v}i_0(s) \quad (5.18)$$

$$\Leftrightarrow V_0(s) = \frac{\frac{1}{\alpha_v}(1+sT_{zv})}{s^3\frac{2T_dT_{pv}C}{K_c\alpha_v}+s^2\frac{T_{pv}C}{K_c\alpha_v}+sT_{zv}+1}V_{0ref}(s) - \frac{sT_{pv}(2T_ds+1)}{s^3\frac{2T_dT_{pv}C}{K_c\alpha_v}+s^2\frac{T_{pv}C}{K_c\alpha_v}+sT_{zv}+1}i_0(s)$$

To ensure the design criteria ${b_k}^2 = a_v b_{k-1} b_{k+1}$, applied to the denominator of (5.18), the values of T_{pv} and T_{zv} can be obtained [12].

$$\begin{cases} {T_{zv}}^2 = a_v\frac{T_{pv}C}{K_c\alpha_v} \\ \left(\frac{T_{pv}C}{K_c\alpha_v}\right)^2 = a_vT_{zv}\frac{2T_dT_{pv}C}{K_c\alpha_v} \end{cases} \Rightarrow \begin{cases} \frac{T_{pv}C}{K_c\alpha_v} = \frac{{T_{zv}}^2}{a_v} \\ \left(\frac{{T_{zv}}^2}{a_v}\right)^2 = a_vT_{zv}2T_d\frac{{T_{zv}}^2}{a_v} \end{cases} \Rightarrow$$
$$\begin{cases} 4{a_v}^4{T_d}^2 = \alpha_v\frac{T_{pv}C}{K_c\alpha_v} \\ T_{zv} = 2{a_v}^2T_d \end{cases} \Rightarrow \begin{cases} T_{pv} = \frac{4{a_v}^3{T_d}^2K_c\alpha_v}{C} \\ T_{zv} = 2{a_v}^2T_d \end{cases} \quad (5.19)$$

Where, $\alpha_v = 3$ and $K_c = 1$.

The linear voltage controller of the DC-DC converter can be represented by the Fig. 5.9.

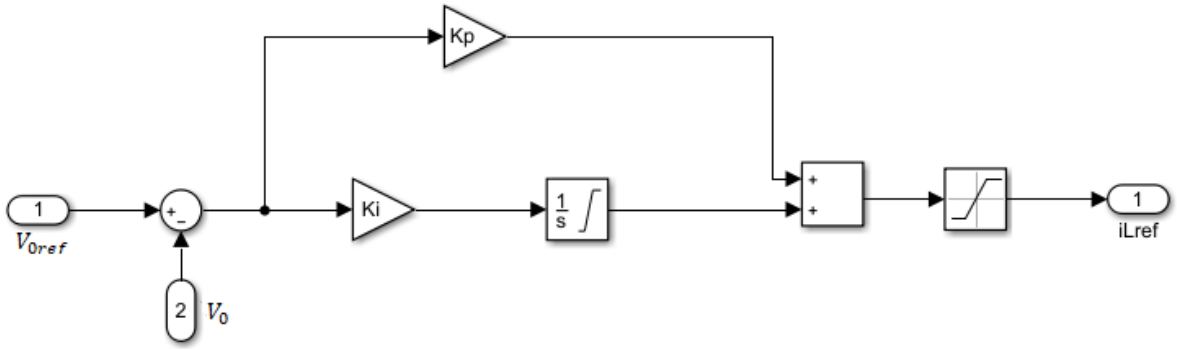

Figure 5.9 – Linear voltage controller of the DC-DC converter representation

The current i_{Lref} present in the Fig. 5.9 will be used in the linear current controller.

Chapter 6

Analysis of Simulation Results

The objectives of this chapter are 1) to simulate the nonlinear and linear controllers, explained in the previous chapters in the context of the described network (chapter 2) and 2) to analyse the obtained results. Moreover, the purpose is to compare results from nonlinear and linear controllers to figure out which is the best solution.

In order to do the simulation a model of the multiterminal HVDC network including the before mentioned controllers was created in MATLAB/Simulink. All the values used in the grid are described in the tables 6.1, 6.2 and 6.3.

Table 6.1 – Simulation parameters of the inverter

Inverter									
$\boldsymbol{\omega_f[rad/s]}$	$f[Hz]$	$S_{cc}[MVA]$	$R_1[\Omega]$	$L_0[mH]$	$R_2[\Omega]$	$C_0[\mu F]$	$R_3[m\Omega]$	$L_1[mH]$	$V_{nac}[kV]$
$6000\boldsymbol{\pi}$	50	1500	0.4	9.2	108.8	0.5	1	2.4	66

Table 6.2 – Simulation parameters of the π line

$\boldsymbol{\pi}$ **Line**						
$\boldsymbol{r[k\Omega]}$	$C_i[\mu F]$	$R_{dc}[\Omega/km]$	$L_{dc}[mH/km]$	$C_{dc}[\mu F/km]$	$d[km]$	$r_{PL}[k\Omega]$
450	24.178	0.0205	0.352	0.233	220	2.757

Table 6.3 – Simulation parameters of the DC-DC converter

DC-DC Converter			
$\boldsymbol{V_n[kV]}$	$I_n[A]$	$C[\mu F]$	$L[mH]$
150	1088	3	17.5

At $t = 0s$, the converters and power lines shown in Fig. 2.1 are in steady state with nominal operating values, except when said otherwise. Moreover, to evaluate the performance of the four terminal HVDC grid under large variation of power, at $t = 0.1s$ two constant power loads are connected into the grid, (one in each independent network), each one of them with half of the nominal power.

6.1 Nonlinear Controllers Simulation Results

In this section all the controllers are nonlinear as was explained in the chapter 4. At $t = 0.1s$ two constant power loads are connected into the grid. All the simulations have the duration of 0.8s.

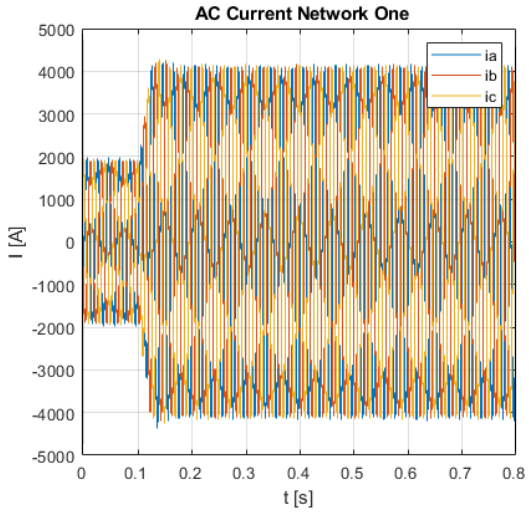

Figure 6.1 – Currents measured on the AC side of network one with nonlinear controller

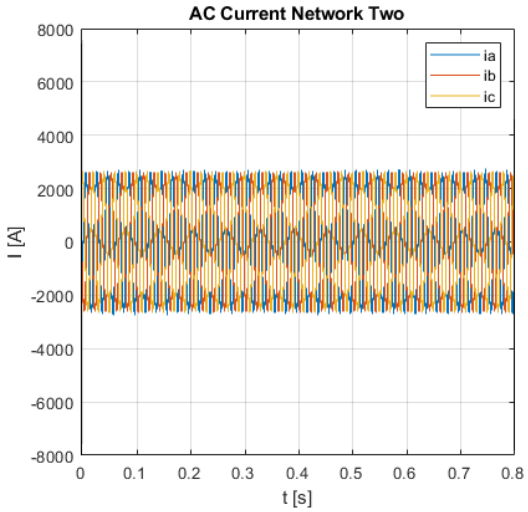

Figure 6.2 – Currents measured on the AC side of network two with nonlinear controller

In Fig. 6.1 it is possible to see the evolution of the AC currents over time in the network one. The currents at $t = 0s$ up to $t = 0.1s$ have the same Root Mean Square (RMS) value which is constant. After that, the currents have a big increase because at that time the constant power loads are connected to the grid, with the system power also increasing, so that RMS value of AC currents has to increase as well due to the response of the line voltage controllers that increase the virtual current to maintain the line voltage. The RMS value of AC currents presented in the Fig. 6.2 don't increase when the constant power loads are connected, because the network two is power controlled and the power reference has to be kept constant (for wind or solar applications). Therefore, the increase of power in the network two due to the electronic load has to be supplied by the interconnecting line two.

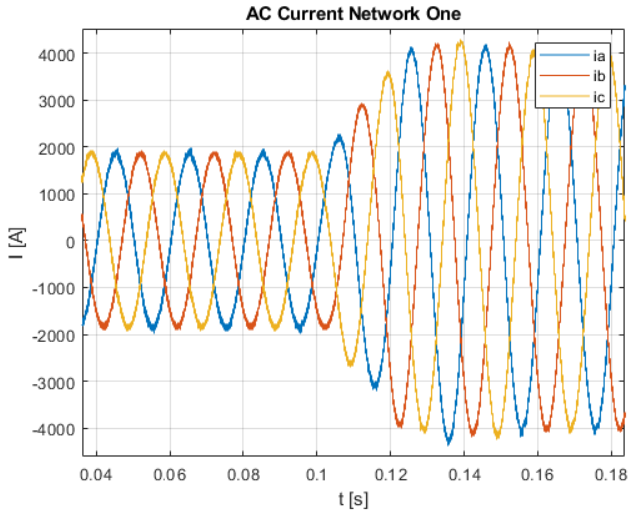

Figure 6.3 – Currents measured on the AC side of network one with nonlinear controller (zoom)

Fig. 6.3 presents a zoom in the AC currents waveform of network one to see their balanced sinusoidal behaviour.

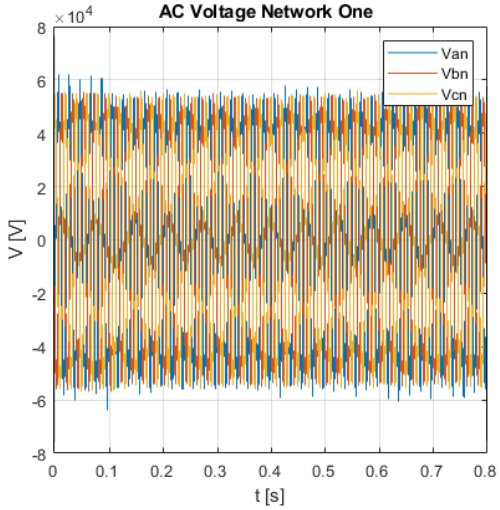

Figure 6.4 – Voltages measured on the AC side of network one with nonlinear controller

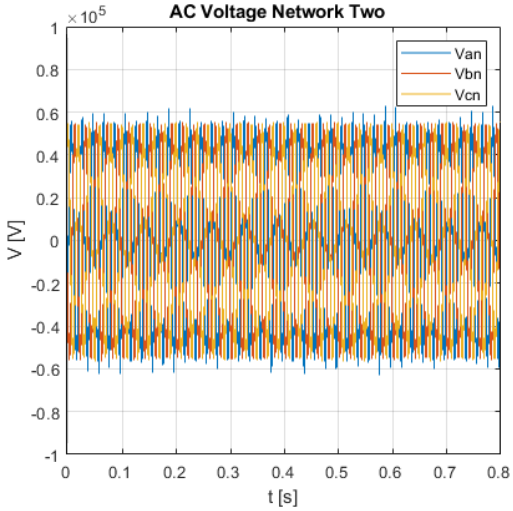

Figure 6.5 – Voltages measured on the AC side of network two with nonlinear controller

The evolution of the AC voltages in both networks, at the input of the LCL filter, as shown in figures 6.4 and 6.5, have constant RMS values over the simulation time and have the nearly the same peak value. This peak value is computed as follows:

$$V_{anpeak} = V_{bnpeak} = V_{cnpeak} = \frac{V_{nac}}{\sqrt{3}}\sqrt{2} \tag{6.1}$$

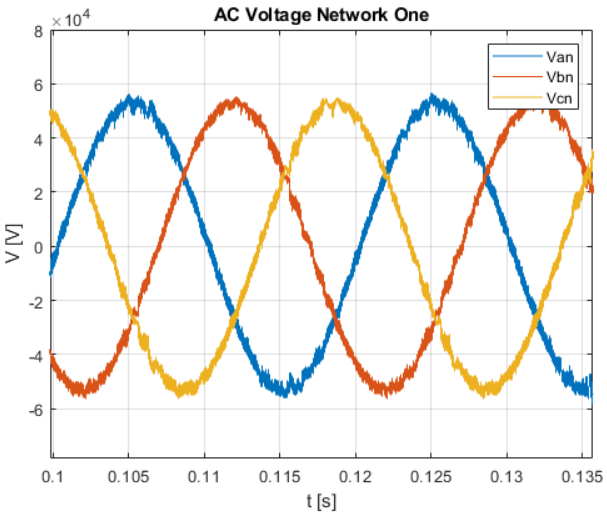

Figure 6.6 – Voltages measured on the AC side of network one with nonlinear controller (zoom)

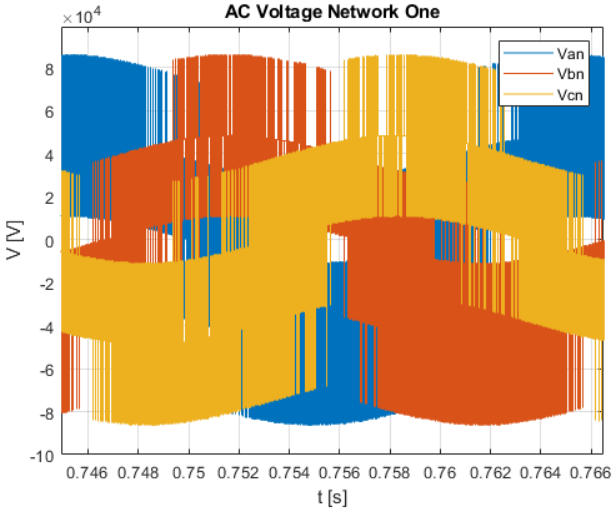

Figure 6.7 – Voltages measured on the AC side of network one with nonlinear controller without the LCL filter (zoom)

For a three-phase system to be balanced, all the source voltages must have the same magnitude and there must be exactly 120 degrees out of phase with one another, then it must be a 120-degree phase difference. Fig. 6.6 confirms that the AC source is a balanced three-phase system. The influence of the LCL filter is also shown in the same figure when compared with Fig. 6.7, because the waveform high frequency harmonics have highly reduced amplitude, otherwise the waveforms would show higher ripple.

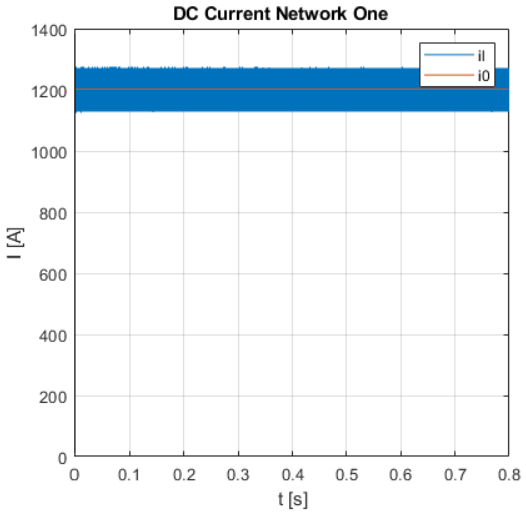

Figure 6.8 – Currents measured on the output DC side of network one with nonlinear controller

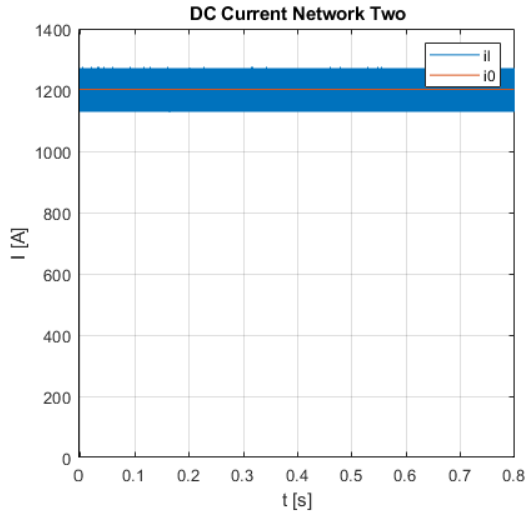

Figure 6.9 – Currents measured on the output DC side of network two with nonlinear controller

The output currents in the figures 6.8 and 6.9 have the same behaviour as expected, because the two networks have similar parameters and have the same type of controllers. The output current i_0 in both networks has average value equal to 1200A because the constant current load imposes that value. In other hand the ripple current in inductor L, i_L has a triangle waveform as expected. This behaviour is possible to see in Fig. 6.10.

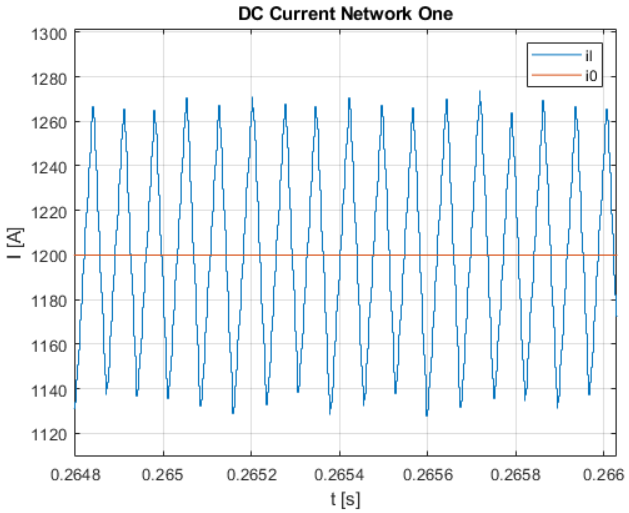

Figure 6.10 – Currents measured on the output DC side of network one with nonlinear controller (zoom)

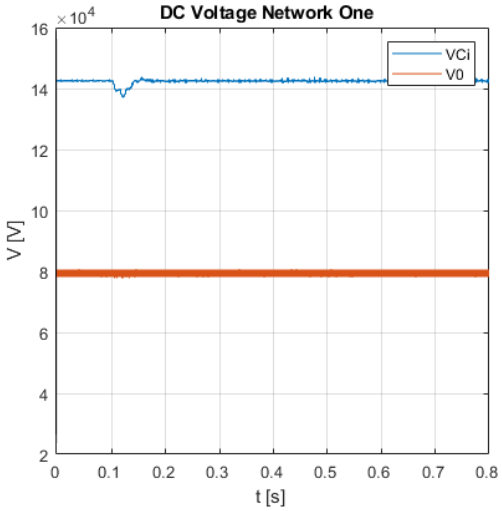

Figure 6.11 – Voltages measured on the DC side of network one with nonlinear controller

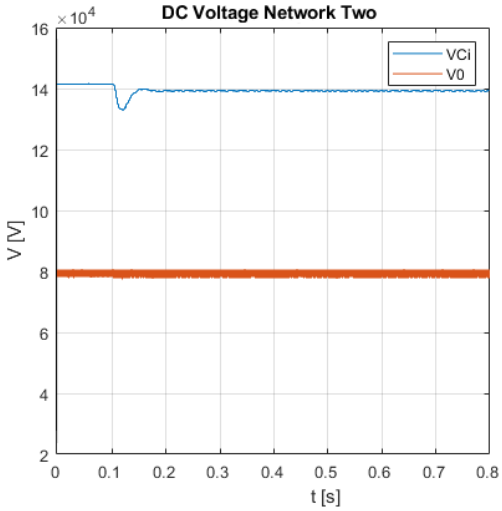

Figure 6.12 – Voltages measured on the DC side of network two with nonlinear controller

The V_{Ci} is the DC voltage at the DC side of the inverter-rectifier and the V_0 is the DC voltage at the output of the network, as shown in the Fig. 2.13. From figures 6.11 and 6.12 it is seen that the nonlinear controllers, at $t = 0.1s$, after a brief transient maintain the grid voltage in droop mode when the constant power loads are connected to the grid. Hence, the V_{ci} voltage droops, but after that the controller rises the voltage to a value slight lower than the rated value. However, in the network two (Fig. 6.12) the error is greater. This happens because in this network only the injected power is controlled not the line voltage. It is possible to minimize this error injecting more power, but in this case extra power, if available, is not strictly needed as the deviation from the rated voltage is not significant. In the network one the voltage drops 5.6 kV approximately; in the second network the voltage drops 8.6 kV (≈ -5%). In other hand, the electronic load voltage V_0 is always equal to 80 kV as expected, showing no voltage oscillations. Moreover, in the figures 6.13 and 6.14 is expressed the same test but without the droop control action. It is seen the line voltage returns to 150 kV not depending on that disturbance.

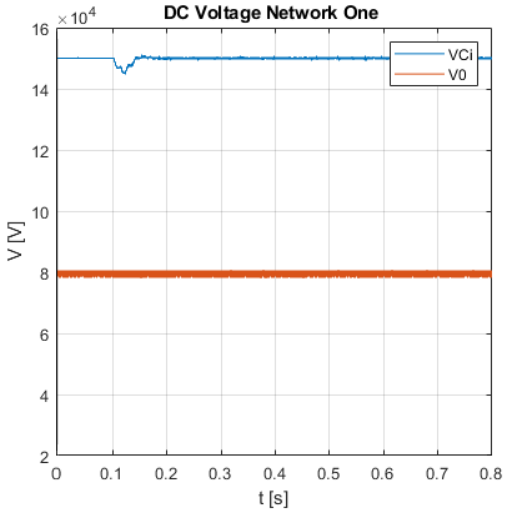

Figure 6.13 – Voltages measured on the DC side of network one with nonlinear controller without droop control

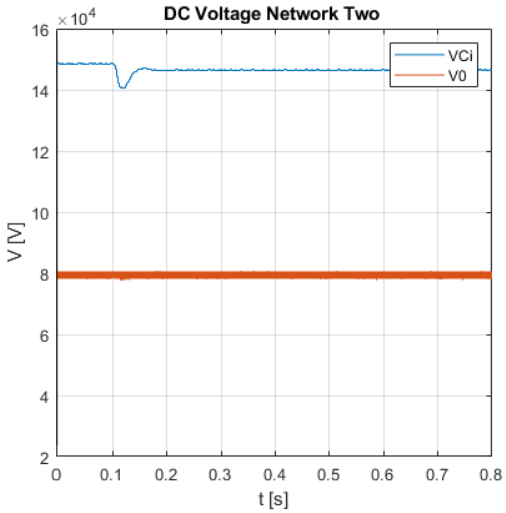

Figure 6.14 – Voltages measured on the DC side of network two with nonlinear controller without droop control

6.2 Linear Controllers Simulation Results

To perform the simulations using linear controllers the multiterminal network has the same topology and parameters. The controllers are linear, except the current controller of the inverter-rectifier which is a sliding mode current controller (nonlinear controller). All the simulations have the duration of 0.8s. The computed gains expressed in the chapter five are shown in the table 6.4 and 6.5.

Table 6.4 – General gains of the PI controllers

$\boldsymbol{\alpha_v}$	$\boldsymbol{\alpha_i}$	$\boldsymbol{a_v}$	$\boldsymbol{a_i}$	$\boldsymbol{K_c}$
1	1	3	3	1

Table 6.5 – PI current and voltage controllers' gains

Inverter			**DC-DC Converter**			
Voltage linear controller			Voltage linear controller		Current linear controller	
$\boldsymbol{K_{pv}}$	K_{iv}	K_w	K_p	K_i	K_{pi}	K_{ii}
-0.094	-50.23	50.23	0.015	25.042	0.012	38.91

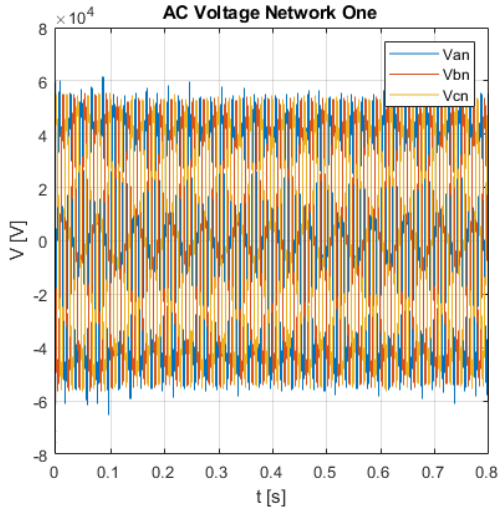

Figure 6.15 – Voltages measured on the AC side of network one with linear controller

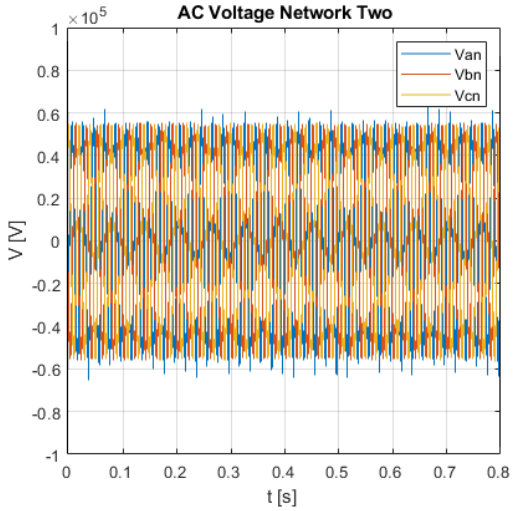

Figure 6.16 – Voltages measured on the AC side of network two with linear controller

From the figures 6.4, 6.5, 6.15 and 6.16 it is seen that the behaviour of the AC voltages in both networks is very similar because the current controller is nonlinear in both cases. Therefore, for this system the use of the nonlinear voltage controller does not represent a significant improvement, when using the nonlinear current controller, as the nonlinear controller is equivalent to a PI controller. The AC currents waveforms are the same as in the previous section because the current controller used is the nonlinear sliding mode current controller. Nevertheless, slightly higher distortion on voltages can be seen in Fig. 6.17.

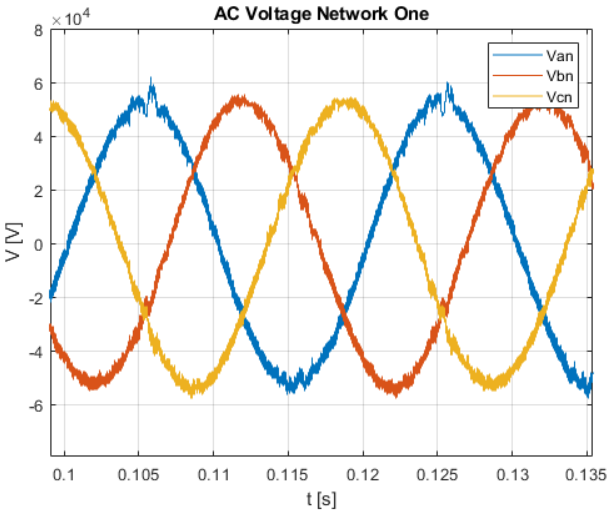

Figure 6.17 – Voltages measured on the AC side of network one with linear controller (zoom)

Comparing the figures 6.6 and 6.17, the utilization of a linear voltage controller doesn't introduce significant harmonic amplitude on high frequencies to the waveform and the system is balanced as well. However, the linear controller presents less harmonic attenuation of high frequencies compared to the nonlinear one. Therefore, it is better to use the nonlinear controller. Moreover, from the Fig. 6.18 is possible to see that the presence of the LCL filter is crucial to attenuate harmonic amplitude on high frequencies of the five levels line to neutral voltages.

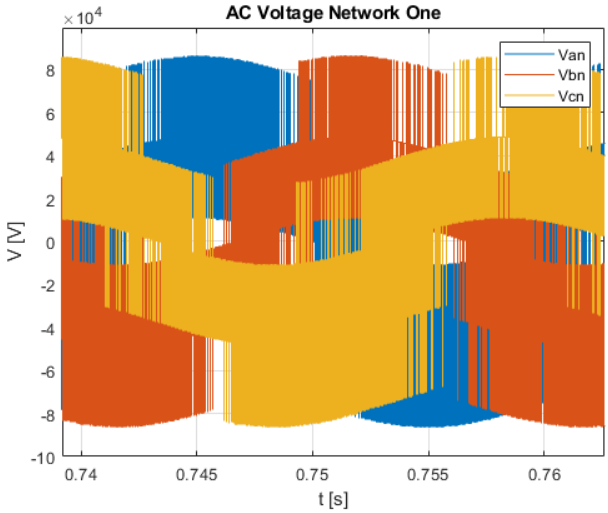

Figure 6.18 – Voltages measured on the AC side of network one with linear controller without LCL filter (zoom)

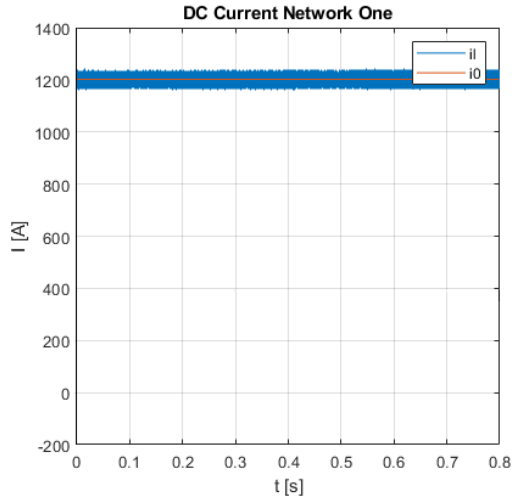

Figure 6.19 – Currents measured on the DC side of network one with linear controller

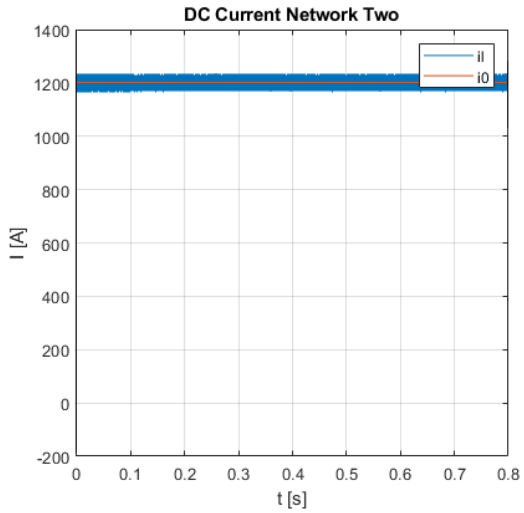

Figure 6.20 – Currents measured on the DC side of network two with linear controller

Considering the figures 6.8, 6.9, 6.19 and 6.20 the behaviour of the DC currents is similar, but the switching frequency is higher and therefore the ripple is smaller.

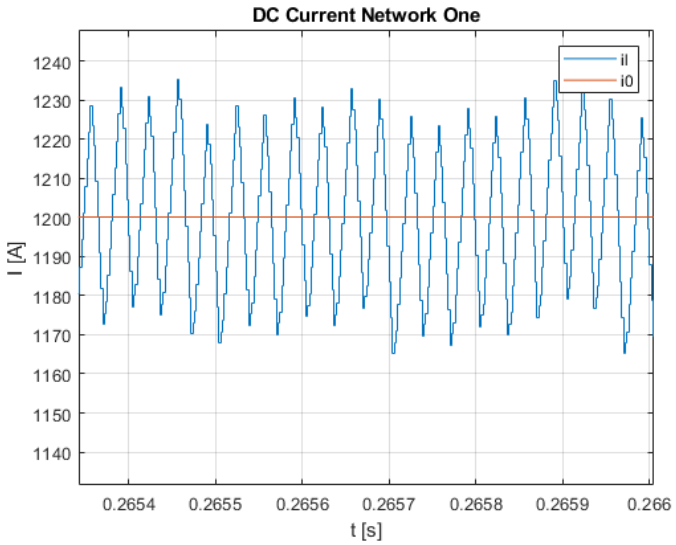

Figure 6.21 – Currents measured on the DC side of network one with linear controller zoom

Comparing figures 6.10 and 6.21, which are zooms of the DC currents for a better visualization of the behaviour of the DC currents. It is seen that the currents are controlled independently of the type of the controller, but the linear voltage controller enables a higher switching frequency, the current showing less ripple.

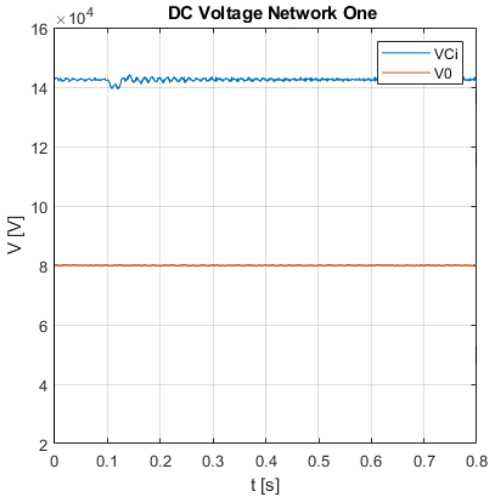

Figure 6.22 – Voltages measured on the DC side of network one with linear controller

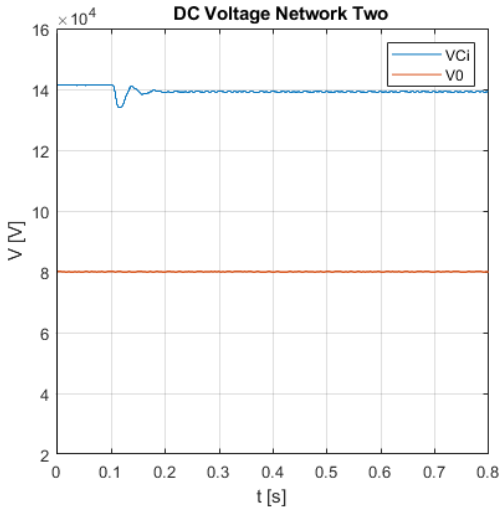

Figure 6.23 – Voltages measured on the DC side of network two with linear controller

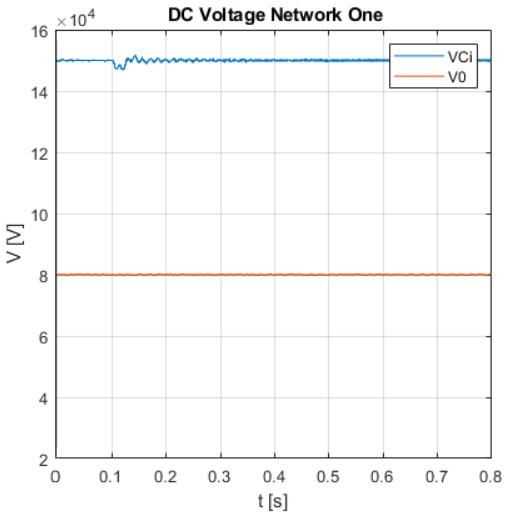

Figure 6.24 – Voltages measured on the DC side of network one with linear controller without droop control

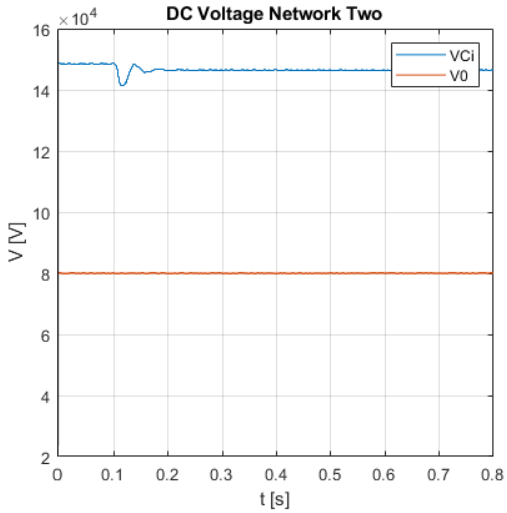

Figure 6.25 – Voltages measured on the DC side of network two with linear controller without droop control

From figures 6.22 and 6.23 it is seen that the linear controllers are subject to a disturbance at $t = 0.1s$ when the constant power loads are connected to the grid. First the V_{ci} voltage droops but after that the controller rises the AC RMS current and the voltage almost returns to the original value. The error in the network two is greater as was explained before. In the network one the voltage drops 2.9 kV approximately; in the second network the voltage drops 7.5 kV. From the figures 6.24 and 6.25 is possible to see the same controllers but without the droop control. In other hand, the V_0 is always equal to 80 kV as expected and does not show voltage oscillations as it is not subjected to load disturbances. However, despite the linear voltage controller being able to overcome the disturbance, comparing the nonlinear controller with the linear it is possible to see that the voltage V_{ci} with linear controller has a slightly more oscillatory behaviour. Therefore, it is better to use the nonlinear controllers for this type of application. For a better understanding of this oscillatory behaviour, Fig. 6.26 shows a zoom of the V_{ci} voltage in network one using the linear controller, while in Fig. 6.27 the same test was done using a nonlinear controller, in order to compare them.

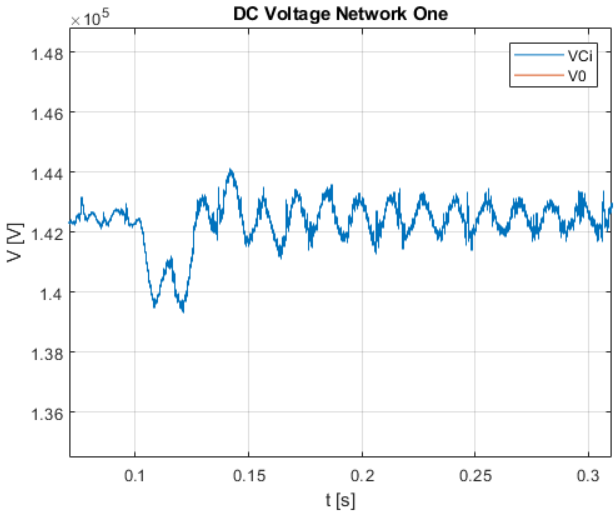

Figure 6.26 – V_{ci} voltage measured on the DC side of network one with linear controller (zoom)

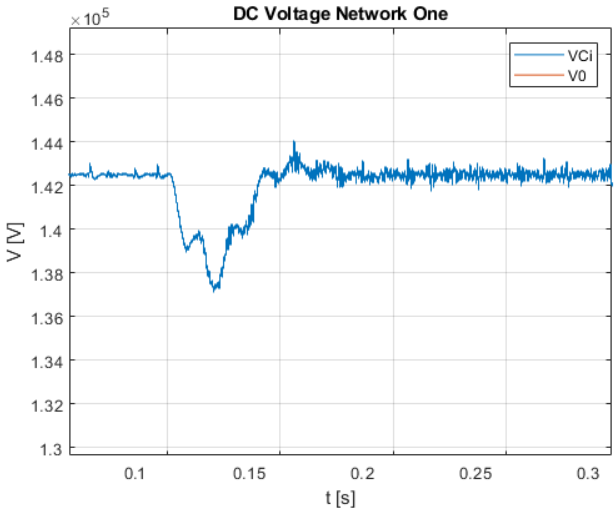

Figure 6.27 – V_{ci} voltage measured on the DC side of network one with nonlinear controller (zoom)

6.3 THD Analysis

The type of network discussed in this dissertation is supplied by high voltage in the AC side, where the total harmonic distortion (THD) must be smaller than 5%. Therefore, in this section a THD analysis is made to check if the THD in the multiterminal network presents acceptable values. To perform this analysis the FFT analysis tool of MATALAB/Simulink is used. All studies were made using a fundamental frequency of 50 Hz with while sampling 5 cycles.

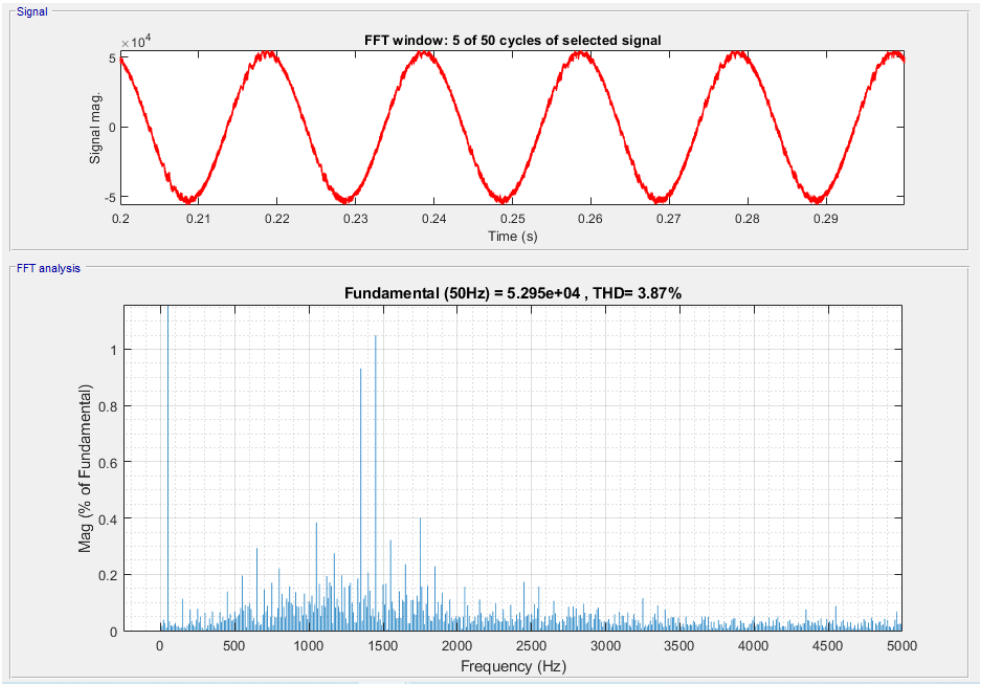

Figure 6.28 – AC Voltage FFT analysis network one using nonlinear controllers

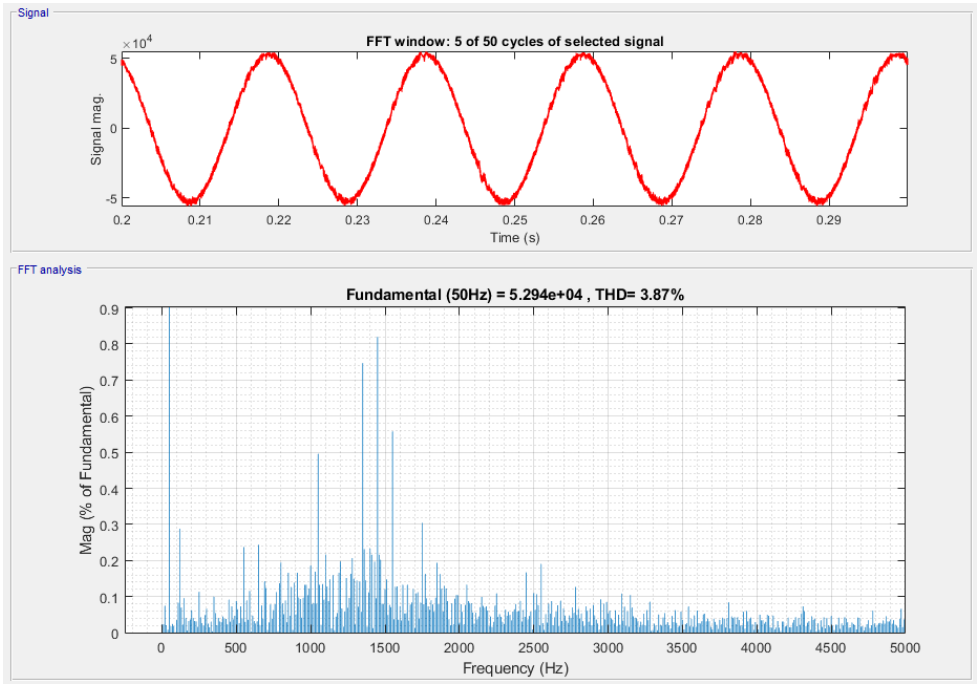

Figure 6.29 – AC Voltage FFT analysis network one using linear controllers

From figures 6.28 and 6.29 it is concluded that the THD of the AC voltage in network one is less than 5% and equal to 3.87% independently of the type of controller.

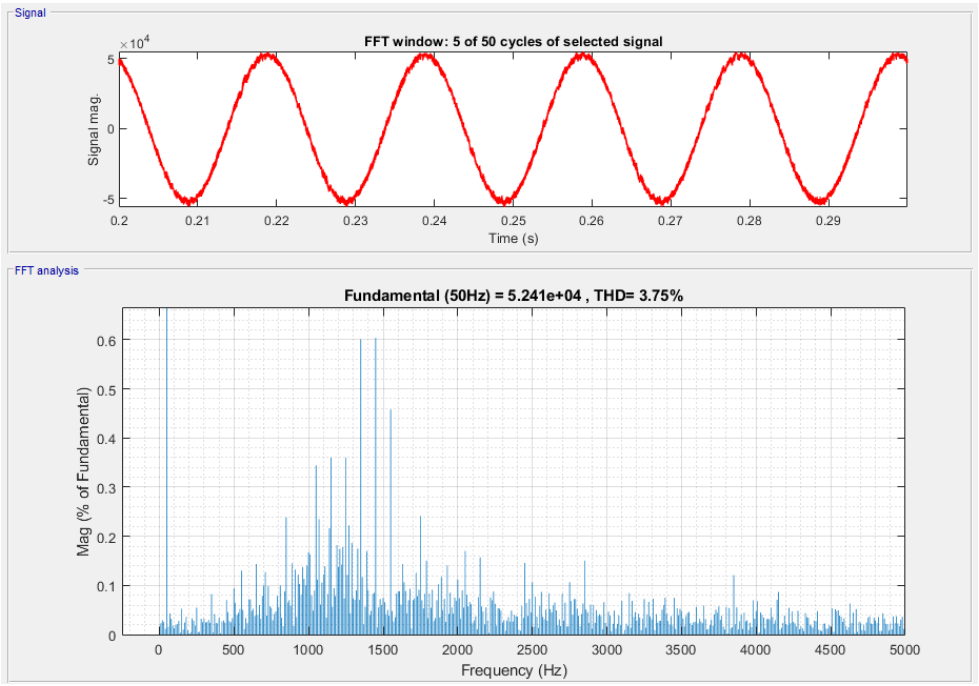

Figure 6.30 – AC Voltage FFT analysis network two using nonlinear controllers

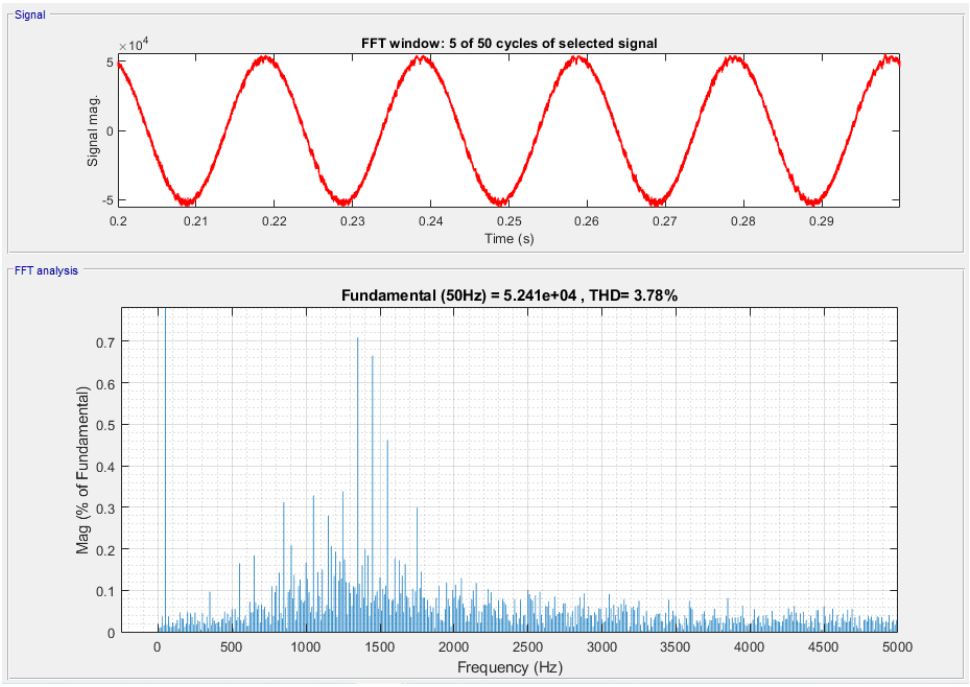

Figure 6.31 – AC Voltage FFT analysis network two using linear controllers

In the case of network two the THD of AC voltage is equal to 3.75% with nonlinear controllers and 3.78% with linear voltage controller (figures 6.30 and 6.31). Therefore, the THD in both cases is less than 5%, being in this test marginally smaller for nonlinear controllers.

Performing the FFT analysis of AC current to both cases (nonlinear and linear controllers) may not be significant because the current controller is nonlinear in both cases. FFT analysis were made to network one and two using nonlinear controllers.

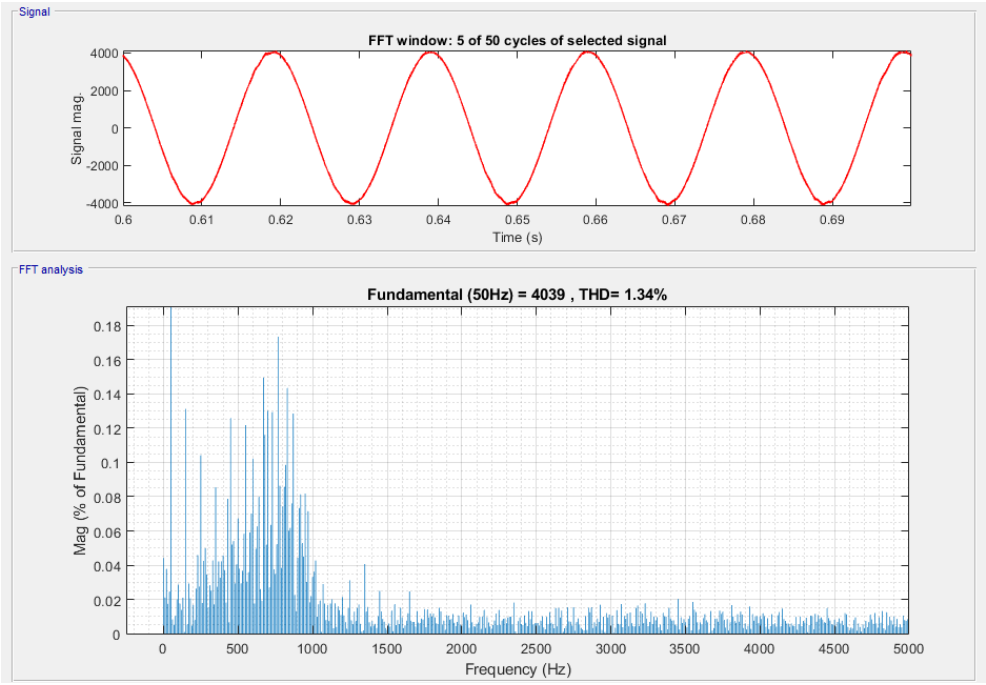

Figure 6.32 – AC current FFT analysis network one using nonlinear controllers

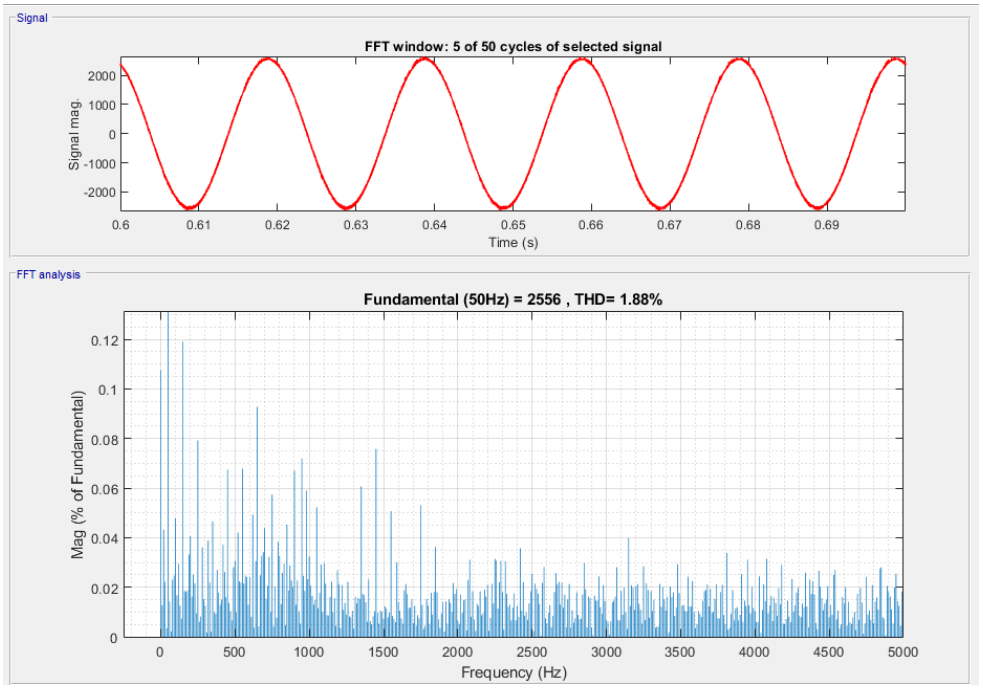

Figure 6.33 – AC current FFT analysis network two using nonlinear controllers

The THD of AC currents of the network one is equal to 1.34%, Fig 6.32 and is equal to 1.88% on network two, Fig.6.33, which are low values.

The table 6.6 summarizes the above discussed AC voltages THD, while adding corresponding THD results for DC voltages. It can be seen that the DC voltage THDs are acceptably low.

Table 6.6 – THD values

	THD AC		**THD DC**	
	AC Voltages		V_{ci} Voltage	
	Network 1	Network 2	Network 1	Network 2
Nonlinear Control	3.87%	3.75%	0.199%	0.042%
Linear Control	3.87%	3.78%	0.256%	0.048%

Chapter 7

Conclusions

This master degree dissertation has developed nonlinear voltage controllers to implement in a four-terminal VSC-HVDC standard network. The standard multi-terminal HVDC network is composed by two similar networks that are interconnected by a third line. To model the multiterminal network, lines were represented by their π models, while each network constant power load, current constant load, AC/DC inverter-rectifier and DC/DC converters were modelled using their state-space equations. Due to the topology of the entire network and the presence of constant power loads, two different nonlinear control techniques were developed and implemented to ensure the global stability, overcoming the stability issue possibly caused by constant power loads in the HVDC network. To check the performance of nonlinear controllers, the steadiness of the DC voltage and their transient and dynamic response were evaluated when the constant power loads were connected.

Results were also obtained using PI linear controllers to compare with the nonlinear ones. The linear controllers are more intuitive and simpler to implement than the nonlinear controllers. However, this type of controller presents more probability to fail when the load has large power deviations. To mitigate the happening of this situation a very large DC capacitor is needed, to prevent large voltage variations, therefore maintaining the linear controllers close to their validity region, enabling the reaching of the steady state.

The first nonlinear controller proposed in this dissertation is based on Lyapunov control theory and combines backstepping control with sliding mode control. These controllers coupled to LCL filters, to attenuate high frequency harmonics, have shown good performance with voltage variations less than 5% and THD less than 4%. On the other hand, the PI linear controllers shown also good performances, presenting only slightly higher THDs.

The second nonlinear controller presented in this dissertation is also based on Lyapunov theory but in this case, it is adapted to DC-DC converters. This controller has shown a good performance in terms of stability and response speed to attain the steady state after the disturbances. The linear controller has presented a good performance as well but with a slightly more oscillatory behaviour.

In this dissertation results were obtained with and without droop control. The usual solution for this type of application is the use of droop control. Thus, the reference voltage is dependent on the required active power, which enables a better result in terms of stability because in the multiterminal network power and voltage are controlled.

The AC current THD in network one equals 1.34% while it is 1.88% on network two, using nonlinear current controllers. On the other hand, the AC voltage THD of network one with nonlinear voltage controller is equal to 3.87% and equal to the THD of network two with linear voltage controller. However, on network two the THD is equal to 3.75% with nonlinear voltage controller and 3.78% with the PI controller. Therefore, all THD are small (less than 5 %). Despite the THD being similar in the majority of tests, network two has a smaller AC voltage THD when using the nonlinear voltage controller. The DC voltage THDs are acceptably low and it can be seen that the THDs using nonlinear control are lower than using linear control. Hence, the nonlinear controller should be the chosen.

To sum up, the recommendation of this dissertation is to use nonlinear controllers in four-terminal HVDC network and in general multiterminal HVDC networks. This statement lies on the fact that this controller deals better with large load variations and with constant power loads, which are increasingly common in HVDC grids. The use of nonlinear controller also permits the use of a smaller DC capacitor, which represents savings in costs and volume.

7.1 Future Work

For future work, it would be interesting to study adaptative voltage regulation in multilevel DC networks instead of just study nonlinear voltage regulation in a multiterminal DC network.

It would be also important to develop a multiterminal network with different renewable energy sources with different levels of voltage and to design and implement controllers capable of control these different voltage levels.

It would also be interesting to study a network with more multiterminal ports and more loads.

Moreover, it is of fundamental importance to make a laboratory prototype to test the developed nonlinear controllers and compare their performance to linear controllers.

Bibliography

[1] "san-franciscos-secret-dc-grid @ spectrum.ieee.org." [Online]. Available: https://spectrum.ieee.org/tech-history/dawn-of-electronics/san-franciscos-secret-dc-grid.

[2] D. J. Becker and B. J. Sonnenberg, "400Vdc power distribution: Overcoming the challenges," *INTELEC, Int. Telecommun. Energy Conf.*, 2010, doi: 10.1109/INTLEC.2010.5525660.

[3] P. Peltoniemi and P. Nuutinen, "DC network characteristics and modeling for power distribution," *2013 15th Eur. Conf. Power Electron. Appl. EPE 2013*, 2013, doi: 10.1109/EPE.2013.6634638.

[4] F. D. Bianchi and O. Gomis-Bellmunt, "Droop control design for multi-terminal VSC-HVDC grids based on LMI optimization," *Proc. IEEE Conf. Decis. Control*, pp. 4823–4828, 2011, doi: 10.1109/CDC.2011.6161070.

[5] M. S. Carmeli, D. Forlani, S. Grillo, R. Pinetti, E. Ragaini, and E. Tironi, "A stabilization method for DC networks with constant-power loads," *2012 IEEE Int. Energy Conf. Exhib. ENERGYCON 2012*, pp. 617–622, 2012, doi: 10.1109/EnergyCon.2012.6348226.

[6] H. Wang and M. A. Redfern, "The advantages and disadvantages of using HVDC to interconnect AC networks," *Proc. Univ. Power Eng. Conf.*, pp. 4–8, 2010.

[7] R. A. F. Ferreira, P. G. Barbosa, H. A. C. Braga, and A. A. Ferreira, "Analysis of non-linear adaptive voltage droop control method applied to a grid connected DC microgrid," *2013 Brazilian Power Electron. Conf. COBEP 2013 - Proc.*, pp. 1067–1074, 2013, doi: 10.1109/COBEP.2013.6785247.

[8] M. Madrigal and E. Acha, "Harmonic modelling of voltage source converters for HVDC stations," *IEE Conf. Publ.*, no. 485, pp. 125–131, 2002, doi: 10.1049/cp:20010530.

[9] S. Cole, *Steady-State and Dynamic Modelling of VSC HVDC Systems for Power System Simulation*, no. September. 2010.

[10] S. Sen, K. Yenduri, and P. Sensarma, "Step-by-step design and control of LCL filter based three phase grid-connected inverter," *Proc. IEEE Int. Conf. Ind. Technol.*, pp. 503–508, 2014, doi: 10.1109/ICIT.2014.6894991.

[11] "J.P.S.Paiva, Redes De Energia Eléctrica Uma Análise Sistémica, 4º Edição, IST PRESS." .

[12] J. F. Silva, 'Electrónica Industrial Semicondutores e Conversores de Potência, série Manuais Universitários,' Lisboa, Fundação Calouste Gulbenkian, 2013." .

[13] E. Hossain, R. Perez, A. Nasiri, and S. Padmanaban, "A Comprehensive Review on Constant Power Loads Compensation Techniques," *IEEE Access*, vol. 6, pp. 33285–33305, 2018, doi: 10.1109/ACCESS.2018.2849065.

[14] "J.M.Lemos, Controlo No Espaço De Estados, IST PRESS."

[15] M. N. Aydin and R. Coban, "LMI-based sliding mode control design and experimental application to an electromechanical plant," *Proc. - 2019 6th Int. Conf. Electr. Electron. Eng. ICEEE 2019*, no. 4, pp. 69–72, 2019, doi: 10.1109/ICEEE2019.2019.00021.

[16] H. K. Khalil, Nonlinear Systems, New Jersey, USA: Prentice Hall.

[17] J. F. Silva and S. F. Pinto, “Control methods for switching power converters,” *Power Electron. Handb.*, pp. 935–998, 2007, doi: 10.1016/B978-012088479-7/50052-3.

[18] Z. Sheng and Q. Wei-qi, “Dynamic systems backstepping control for,” pp. 1–20, 2017.

[19] J. Huang, D. Xu, W. Yan, L. Ge, and X. Yuan, “Nonlinear Control of Back-to-Back VSC-HVDC System via Command-Filter Backstepping,” *J. Control Sci. Eng.*, vol. 2017, 2017, doi: 10.1155/2017/7410392.

[20] G. Marques, “Dinâmica das Máquinas Eléctricas,” p. 289, 2002.

[21] F. Silva, S. Pinto, and J. Santana, “Conversores Comutados para Energias Renováveis,” p. 172, 2016, [Online]. Available: https://fenix.tecnico.ulisboa.pt/downloadFile/563568428750567/Livro_CCER_2017.pdf.

[22] M. A. A. Murad and F. Milano, “Modeling and Simulation of PI-Controllers Limiters for the Dynamic Analysis of VSC-Based Devices,” *IEEE Trans. Power Syst.*, vol. 34, no. 5, pp. 3921–3930, 2019, doi: 10.1109/TPWRS.2019.2911034.

[23] A. Platon, S. Oprea, A. Florescu, and S. G. Rosu, “Simple and Digital Implementation of PI Controller Used in Voltage-Mode Control,” *Proc. 10th Int. Conf. Electron. Comput. Artif. Intell. ECAI 2018*, no. 2, 2019, doi: 10.1109/ECAI.2018.8679078.

[24] João.J.E.Santana, “Electrónica de Potência,” Lisboa, Fundação Calouste Gulbenkian**.**

Appendix A

Table A.1 – MATLAB workspace

Variable	Value	Variable	Value
$\boldsymbol{a_i}$	3	$L[mH]$	17.5
$\boldsymbol{\alpha_i}$	1	$L_0[mH]$	9.2
$\boldsymbol{\alpha_v}$	1	$L_1[mH]$	2.4
$\boldsymbol{a_v}$	3	$L_{dc}[mH/km]$	0.352
$\boldsymbol{C[\mu F]}$	3	P[MW]	163.2
$\boldsymbol{C_0[\mu F]}$	0.5	$r[k\Omega]$	450
$\boldsymbol{C_{dc}[\mu F/km]}$	0.233	R_e	4.596×10^{-5}
$\boldsymbol{C_i[\mu F]}$	24.178	$R_1[\Omega]$	0.415
$\boldsymbol{d[km]}$	220	$R_2[\Omega]$	36.277
$\Delta_{iLmax}[\boldsymbol{A}]$	142.763	$R_3[\Omega]$	0.001
$\Delta_{\boldsymbol{u}}[\boldsymbol{V}]$	1500	$R_{dc}[\Omega/km]$	0.0205
$\Delta_{\boldsymbol{V0}}[\boldsymbol{V}]$	750	$r_{pl}[\Omega]$	2757.4
$\boldsymbol{f[Hz]}$	50	$r_{pl1}[\Omega]$	137.87
$\boldsymbol{f_c[Hz]}$	15000	$S_{cc}[MVA]$	1500
$\boldsymbol{G_i}$	-0.359	$T[\mu s]$	66.667
$\boldsymbol{i_L[A]}$	1427.6	T_d	3.333×10^{-5}
$\boldsymbol{I_n[A]}$	1088	T_{dv}	5×10^{-4}
$\boldsymbol{K_c}$	1	T_p	0.0257
$\boldsymbol{K_d}$	15000	T_{pv}	0.0399
$\boldsymbol{K_i}$	25.0420	T_z	3×10^{-4}
$\boldsymbol{K_{ii}}$	38.915	T_{zv}	6×10^{-4}
$\boldsymbol{K_{iv}}$	-50.229	$u_{cmax}[V]$	10
$\boldsymbol{K_p}$	0.0150	$V_0[kV]$	75
$\boldsymbol{K_{pi}}$	0.0117	$V_n[kV]$	150
$\boldsymbol{K_{pv}}$	-0.0945	$V_{nac}[kV]$	66
$\boldsymbol{K_w}$	50.229	$\omega_f[Hz/s]$	1.885×10^4

To size the capacitor C_i of figure 2.13 the following equation were used [24]:

$$C_i = \frac{I_n T}{2\Delta_u} \tag{A.1}$$

Where Δ_u it is considered to be 10% of V_n.

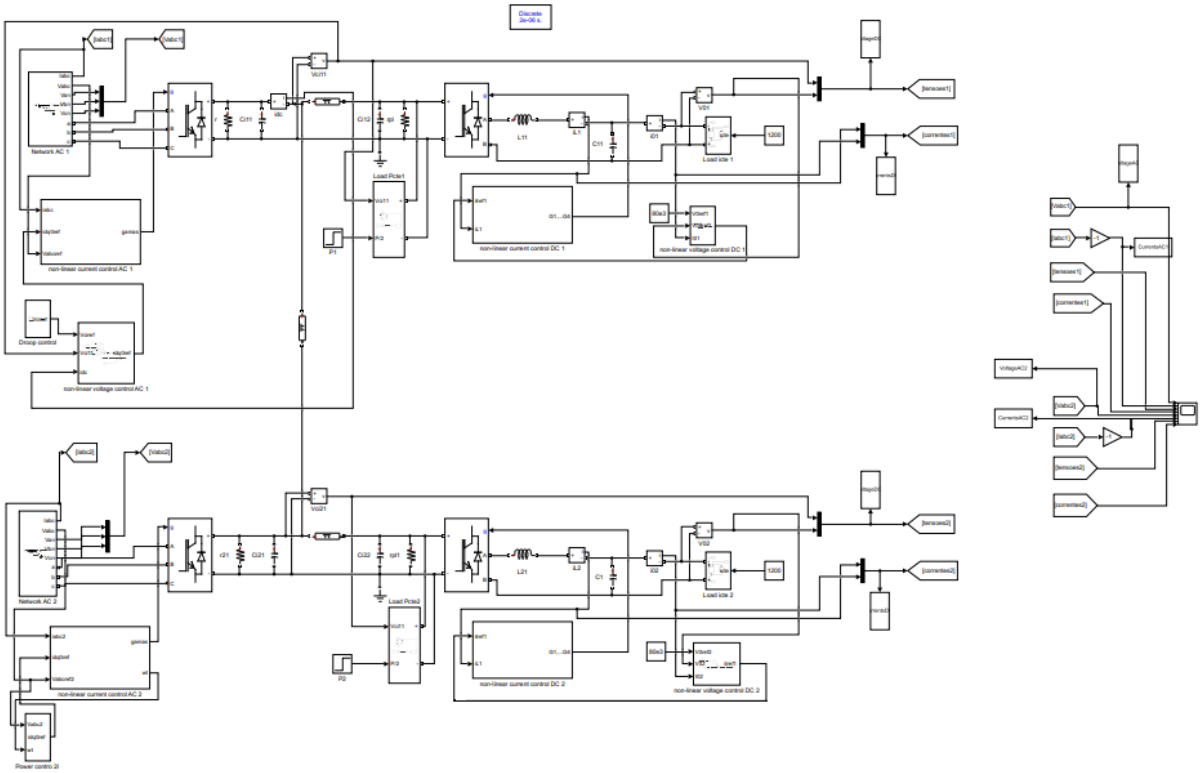

Figure A.1 – Four-terminal VSC-HVDC model with droop control and nonlinear controllers MATLAB/Simulink

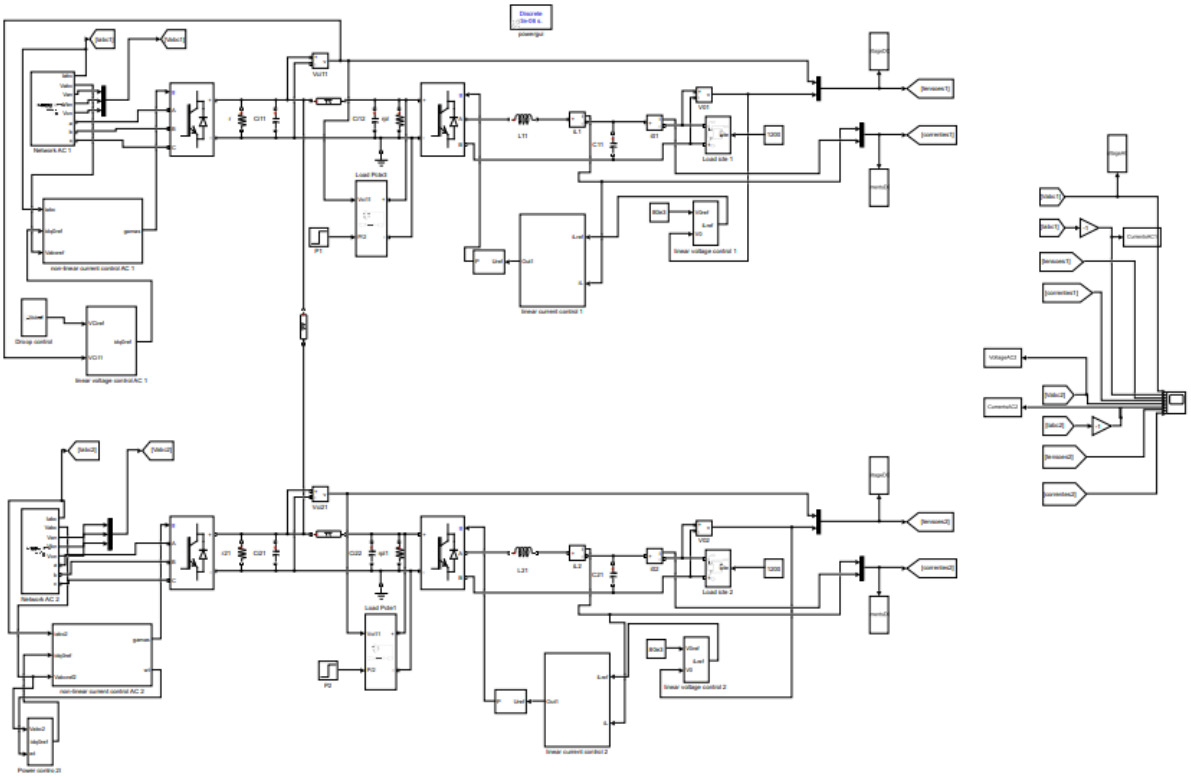

Figure A.2 – Four-terminal VSC-HVDC model with droop control and linear controllers MATLAB/Simulink